Probing the effect of glass network on the synthesis and luminescence properties of composite perovskite glasses

Anna Karagiannaki

Advisory Committee

Stratakis Emmanuel, Research Director, IESL-FORTH, University of Crete (Supervisor)
Athanassios Coutsolelos, Prof. University of Crete (Co-Supervisor)
George Kioseoglou, Prof. University of Crete

Department of Chemistry
University of Crete

March 2022

Διερεύνηση της επίδρασης του πλέγματος στην σύνθεση και φωτοφωταύγεια σύνθετων περοβσκιτικών υάλων

Άννα Καραγιαννάκη

Τριμελής επιτροπή

Εμμανουήλ Στρατάκης, Διευθυντής Ερευνών, IESL-FORTH, Πανεπιστήμιο Κρήτης (Επιβλέπων)
Αθανάσσιος Κουτσολέλος, Prof. Πανεπιστήμιο Κρήτης (Επιβλέπων)
Γεώργιος Κιοσέογλου, Prof. Πανεπιστήμιο Κρήτης

Τμήμα Χημείας
Πανεπιστήμιο Κρήτης

Ηράκλειο,Μάρτιος 2022

Table of content

Acknowledgments

First of all, I would like to express my sincere gratitude to Dr. Emmanuel Stratakis for his continuous support of my Master thesis research, for his guidance and encouragement. His guidance and motivation were very important and crucial to the completion of this thesis. He has also supported me with his immerse knowledge, allowing me to work on my own way, while at the same time showing me how to increase my productivity.

Besides my supervisor, I would like to thank Dr. Ioannis Konidakis, for his daily help, guidance, encouragement and motivation he showed to me, for the greatest possible result and his effort to solve any issue and query throughout my Master thesis. Alexandra Manousaki for the hours spent in Scanning Electron Microscopy, Clyto Katsara for the Raman spectra, George Kourmoulakis and Ioanna Demeridou for the photoluminescence spectra as well as their time invested in talking through the experimental results. I would also like to thank my fellow lab-mates and my colleagues for the support as well as for all the fun we have had during these two years.

I would also like thanks the members of the committee of my thesis Prof. George Kioseoglou and Dr. Athanassios G. Coutsolelos, for doing me the honor of evaluating my Master thesis.

A special thanks to my parents. Words cannot express how grateful I am to my parents for all the sacrifices that they have made on my behalf and encouragement to reach my goals.

Abstract

All-inorganic cesium lead perovskite nanocrystals are highly promising candidates for various optoelectronic and photonic applications. Although, their poor stability upon exposure to moisture as well as the lead toxicity issues limits significantly their use. A modern and promising strategy on resolving these issues is the encapsulation of highly luminescent perovskite nanocrystals within transparent inorganic oxide glasses. While the encapsulation procedure effect on the development and properties of the so-formed PV-Glasses has been explored in detail, there is luck of understanding the influence of the selected glass composition and network type on the outcome of the perovskite-glass development. In this study, we report on the synthesis and photoluminescence properties of composite perovskite-glasses upon growing all-inorganic lead halide perovskites within three different types of inorganic oxide glasses. In particular, silver metaphosphate glass is selected as the first host. It is revealed that the low glass transition temperature of the phosphate glass limits significantly the temperature range of the required post-melting annealing treatment, while the lead salt precursors react with the phosphate entities of the network and destroying the stoichiometry of the PNCs. As a result, the formation of PNCs is hindered. Following this, a double network former borophosphate glass was employed. While annealing treatments at higher temperature were facilitated in this case, the high silver content becomes an obstacle for the perovskite formation. The last composite glass studied, is a borate system with lead bromide ($CsPbBr_3$) and cesium lead iodide ($CsPbI_3$) perovskites. The developed composite glasses exhibit interesting photoluminescence features, while the interactions with the borate network are thoroughly investigated.

Περίληψη

Οι πλήρως ανόργανοι νανοκρύσταλλοι περοβσκίτη μολύβδου καισίου είναι πολλά υποσχόμενοι υποψήφιοι για διάφορες οπτοηλεκτρονικές και φωτονικές εφαρμογές. Αν και η αστάθεια τους κατά την έκθεση στην υγρασία καθώς και η τοξικότητας του μολύβδου περιορίζουν σημαντικά τη χρήση τους. Μια σύγχρονη και πολλά υποσχόμενη στρατηγική για την επίλυση αυτών των προβλημάτων είναι η ενθυλάκωση νανοκρυστάλλων περοβσκίτη υψηλής φωταύγειας μέσα σε διαφανή γυαλιά. Η επίδραση της διαδικασίας ενθυλάκωσης στην ανάπτυξη και τις ιδιότητες των σχηματισμένων ΠΒ-Υάλων έχει διερευνηθεί λεπτομερώς, υπάρχει όμως η ανάγκη να κατανοήσουμε την επίδραση της επιλεγμένης σύνθεσης γυαλιού και του τύπου δικτύου στο αποτέλεσμα της ανάπτυξης περοβσκιτικών υάλων. Σε αυτή τη μελέτη, αναφέρουμε τις ιδιότητες σύνθεσης και φωτοφωταύγειας των σύνθετων υάλων περοβσκίτη κατά την ανάπτυξη εξ ολοκλήρου ανόργανων περοβσκιτών αλογονιδίου μολύβδου εντός τριών διαφορετικών τύπων γυαλιών ανόργανου οξειδίου. Συγκεκριμένα, το γυαλί μεταφωσφορικού αργύρου επιλέγεται ως πρώτος ξενιστής. Αποκαλύπτεται ότι η χαμηλή θερμοκρασία υαλώδους μετάπτωσης του φωσφορικού γυαλιού περιορίζει σημαντικά το εύρος απαιτούμενης θερμοκρασίας για την ανάπτυξη των περοβσκιτών, ενώ τα άλατα μολύβδου αντιδρούν με τις φωσφορικές οντότητες του δικτύου και καταστρέφουν τη στοιχειομετρία των PNC. Ως αποτέλεσμα, παρεμποδίζεται ο σχηματισμός PNC. Μετά από αυτό, χρησιμοποιήθηκε ένα διπλό δίκτυο βοροφωσφορικού υάλου. Ενώ σε αυτήν την περίπτωση διευκολύνθηκαν οι διεργασίες ανάπτυξης σε υψηλότερη θερμοκρασία, η υψηλή περιεκτικότητα σε άργυρο αποτελεί εμπόδιο για το σχηματισμό περοβσκίτη. Το τελευταίο σύνθετο γυαλί που μελετήθηκε, είναι ένα βορικό σύστημα με περοβσκίτες βρωμιούχου μολύβδου ($CsPbBr_3$) και ιωδιούχου μολύβδου ($CsPbI_3$). Τα αναπτυγμένα σύνθετα γυαλιά παρουσιάζουν ενδιαφέροντα χαρακτηριστικά φωτοφωταύγειας, ενώ οι αλληλεπιδράσεις με το βορικό δίκτυο διερευνώνται διεξοδικά.

List of Figures

Fig. 15: Normalized room temperature Raman spectra of the pristine $AgPO_3$ glass, the perovskite glasses $0.1CsPbBr_3$-$0.9AgPO_3$ and $0.1CsPbI_3$-$0.9AgPO_3$, respectively.

Fig. 16: (a), (b) Room temperature photoluminescence (PL) spectra, for the sake of comparison the PL spectra of the non-encapsulated PV NCs are added in (b) and (c) XRD patterns of pristine $AgPO_3$ glass and the PV-Glasses[87].

Fig. 17: Optical absorbance spectra of pristine $AgPO_3$ glass and composite glasses.

Fig. 18: Pictures of (a) $0.1CsPbI_3$-$0.9(0.5Ag_2O$-$0.3B_2O_3$-$0.2P_2O_5)$ composite glass after quenching, and (b) after 3 hours of annealing at 320 ^oC. (c) Indicative room temperature photoluminescence (PL) spectra[87].

Fig. 19: Room temperature photoluminescence (PL) spectra of (a) $0.05CsPbBr_3$-$0.95(0.25Na_2O$-$0.75B_2O_3)$, and (b) $0.1CsPbBr_3$-$0.9(0.25Na_2O$-$0.75B_2O_3)$ composite glasses after 10 hours of annealing at 700^oC. The inset of (a) show a picture of the former glass under UV light irradiation. The inset of (b) depicts the corresponding optical absorbance profiles of the composite PV-Glasses and the pristine sodium borate glass, while the PL of the $0.1CsPbBr_3$ PV-Glass is also included. PL spectra of (c) $0.05CsPbBr_3$-$0.95(0.25Na_2O$-$0.75B_2O_3)$, and (d) $0.1CsPbBr_3$-$0.9(0.25Na_2O$-$0.75B_2O_3)$ composite glasses after 10 hours of annealing at various temperatures (600, 700, 800^oC). The corresponding spectra of the pristine $0.25Na_2O$-$0.75B_2O_3$ glass is also shown at both spectra[87].

Fig. 20: Transmission electron microscopy (TEM) images of cesium lead bromide PNCs within $0.05CsPbBr_3$-$0.95(0.25Na_2O$-$0.75B_2O_3)$ glass (a and b), and within $0.1CsPbBr_3$-$0.1(0.25Na_2O$-$0.75B_2O_3)$ glass (c and d). (e) Histograms of PNCs size distribution in PV-Glasses[87].

Fig. 21. Room temperature Raman spectra of the two composite PV-Glasses and the pristine $0.25Na_2O$-$0.75B_2O_3$ glass[87].

Fig. 22. (a) Room temperature photoluminescence (PL) spectra of $0.1CsPbI_3$-$0.9(0.25Na_2O$-$0.75B_2O_3)$ composite glass after 8 hours of annealing at 700 ^oC. The inset of (a) shows the corresponding optical absorbance profiles of the composite $CsPbI_3$ PV-Glass and the pristine sodium borate glass, while the PL of the former is also included. (b) Power excitation density dependence of the PL intensity. The inset of (b) shows the PL intensity dependence on the excitation power of a lasing system[87].

Introduction

1.1 Perovskite

Perovskites have emerged as a class of semiconductor materials with unique properties such as tunable bandgap[1,2], high absorption coefficient[3], broad absorption spectrum[4], high charge carrier mobility[5] and long charge diffusion length[6].[7-10] Properties, that arise a broad range of photovoltaic and optoelectronic applications. Some of these applications are solar cells,[11,12] solar-fuel energy conversion devices[13], light emitting diodes[14,15], lasers[16,17], water splitting[18], etc. It is now considered to be one of the most promising material in optoelectronics because of its low cost, high performance and abundance. Unlike traditional semiconductors, there can be different combinations for the perovskite composition with easy synthetic routs. There can have tunability of the characteristics of the material such as band-gap, conductivity, mobility, etc., by changing the composition, a characteristic that makes them important for device configuration and optimization.

The term perovskite originates from the first mineral perovskite and was named in honor of the Russian mineralogist Lev Perovski[19]. This was calcium titanate ($CaTiO_3$) and the whole family of material with this particular crystal structure are called perovskites. The synthesis of lead and tin based perovskites came in 1978 by D. Weber and had the following formulas $MAPbX_3$ (MA = CH_3NH_3, X = Cl, Br, and I), $MASnBr_xI_{3-x}$[20,21].

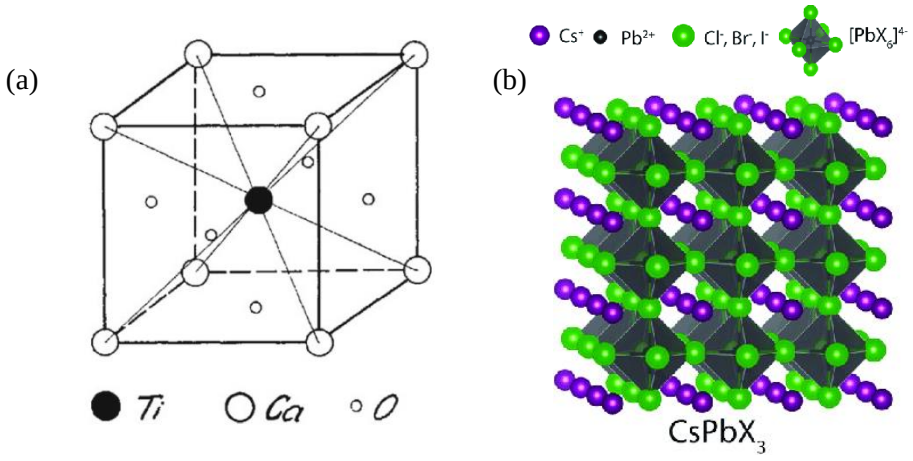

Fig. 1: (a) Basic structural arrangement of the atoms in the mineral perovskite as shown by Thomas Barth in 1925[22], (b) 3D structure of $CsPbX_3$ perovskite[23].

Since then, a great amount of research has been established regarding this type of material and the perovskites have been used in various forms of devices. Although, their physical and chemical properties had not been in depth investigated, this was because there was a lack of potential application[24]. Since 2009[25] that it found application in solar cells the interest of the scientific community has raised regarding perovskites, as it tourns out to be one of the most effective light absorber material for solar cell.

Metal halide perovskites are classified into two categories based on their crystal structure. The first one being the 3D-structured perovskite with the chemical formula ABX_3 and the other one called a 2D-structured perovskite with the formula A_2BX_4. M site is a divalent metal such as Pb^{2+}, Sn^{2+}, Zn^{2+}; X site is a monovalent halide anion (Cl^-, Br^-, or I^-); and A site is a large monovalent cation which can either be inorganic (e.g. Cs^+) or organic (e.g. $CH_3NH_3^+$, $C_4H_9NH_3^+$, C_6H_5-$C_2H_4NH_2^+$, etc.).

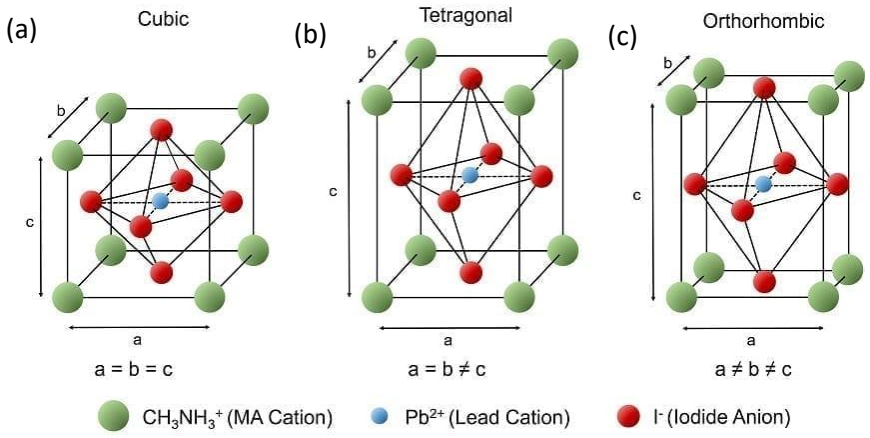

Fig. 2: (a) Crystalline structure of cubic (α phase); (b) crystalline structure of the tetragonal crystal system (β) phase and orthorhombic (γ) phase of $MAPbX_3$[26].

The metal B is surrounded by six halogen atoms in an octahedron structure, and the cation A can be either located in the center of eight BX_6 octahedral network (3D perovskite) as shown in Fig. 1 or either sandwiched between corner-sharing BX_6 octahedral layers (2D perovskite).The crystalline structure of perovskites (ABX_3) in its cubic structure, has the B cation in 6-fold coordination, surrounded by an octahedron of anions, and the A cation in 12-fold cuboctahedral coordination as shown in Fig. 2a. For this structure to be stable in the ideal cubic phase, the tolerance factor t,

should be close in the range of 0.813 and 1.107. Values that are beyond this range are considered thermodynamically unstable accompanied by lattice distortion.

$$t = \frac{r_A + r_X}{\sqrt{2}(r_B + r_X)}$$

where r_A, r_M , and r_X are the ionic radii of the corresponding atoms. As mention above, when the tolerance factor is 1 we have the ideal cubic face, in case it is far from that then the symmetry of the structure is lowered. In order to satisfy the ideal cubic structure, the radii of cation A must be much larger than that of cation B. The atom B is usually lead (Pb) or tin (Sn) which are very big atoms, so the cation A must be huge.

In order for the perovskite crystal structure to remain cubic the tolerance factor must lie between 0.89-1.31. If the tolerance factor is lower than this then the symmetry is lowered and the crystalline structure is tetragonal (β-phase) or orthorhombic (γ-phase) as shown in Fig. 2b and c. If the tolerance factor is larger than 1, it would undermine the 3D B-X network, leading to layered structure perovskite as shown in Fig. 1b. Also, it is possible for the perovskite to undergo phase transition with different temperatures. For example, $CsPbBr_3$ with a tolerance factor of 0.92, has two phase transitions, one takes place at 403 K from a cubic to the tetragonal phase, and the second one at 361 K, from the tetragonal to the orthorhombic phase[27]. This phase transition would affect the thermal stability and performance of perovskite devices. All phase transitions of the cesium lead halides are of antidistortive type and occur due to the condensation of the soft mode at the Brillouin zone boundary, i.e. they are related to octahedral tilting[28].

1.1.1 Optical properties of perovskites

I. Band structure of perovskite

In metal halide perovskites the band structure is predominantly determined by the MX_6 building block. In lead-based perovskites, the valence band (highest occupied molecular orbital, HOMO) is mostly contributed by Pb 6*s*- X *p* σ-antibonding orbitals while the conduction band (lowest

unoccupied molecular orbital, LUMO) is from the Pb 6*p*- X *p* π-antibonding an Pb 6*p*- X *s* σ-antibonding orbitals[29]. The electronic performance of perovskite can be attributed to the lone pair of *s* electrons in Pb cation. As opposed to most metal cations at which the most outer *s* orbitals are empty, Pb has an occupied 6*s* orbital lying below the valence bands[30,31]. The valence band maximum (VBM) has antibonding character of Pb-6*s* and X-*p*, while the conduction band minimum (CBM) is mainly contributed from Pb 6*p* state. These unique characteristics of the perovskite are attributed to the dual nature of electronic structures that have both ionic and covalent characteristics.

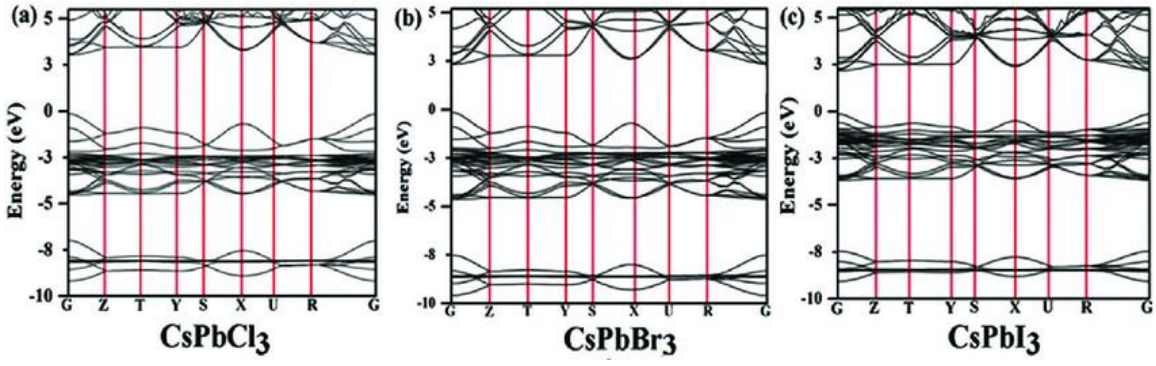

Fig. 3: Electronic band structures of (a) $CsPbCl_3$ (b) $CsPbBr_3$ and (c) $CsPbI_3$[32].

The electronic band structure of perovskite is also responsible for its strong optical absorption property comparing to that of other solar cell absorbers. The absorption coefficient in the visible range of some perovskites is higher than both GaAs and that of silicon, making perovskites useful for solar cells and opto-electronic devises, since less material is needed in optimal absorption[30]. Properties such as high carrier mobility, efficient charge transport, and long carrier diffusion length can as well be attributed to their electronic band structure[33,34].

II. Bandgap tunability

Besides perovskites superior performance in solar cells, they also find application as light emitters diodes as well as lasers[17,35-38]. In comparison with conventional semiconductors, perovskites provide facile tunable emission throughout the whole visible range by controllable stoichiometry as well as control over the nanoparticles size[39,40]. It is possible to have tunability of the emission by substituting halide elements from chloride to iodide. By substituting either mixture of chlorides and bromides, or bromides and iodides, the emission of all inorganic perovskite $CsPbX_3$ (X= Cl, Br, I,

or mixture), can be tuned from 400 nm (blue) to 700 nm (red), which covers the whole visible region as shown in Fig. 4. Also, another way to tune the emission is by replacing the lead with other kinds of metal ions, or by inserting other kind of organic molecules. It is also possible, to tune the perovskite emission to near infrared or ultraviolet region[35,41].

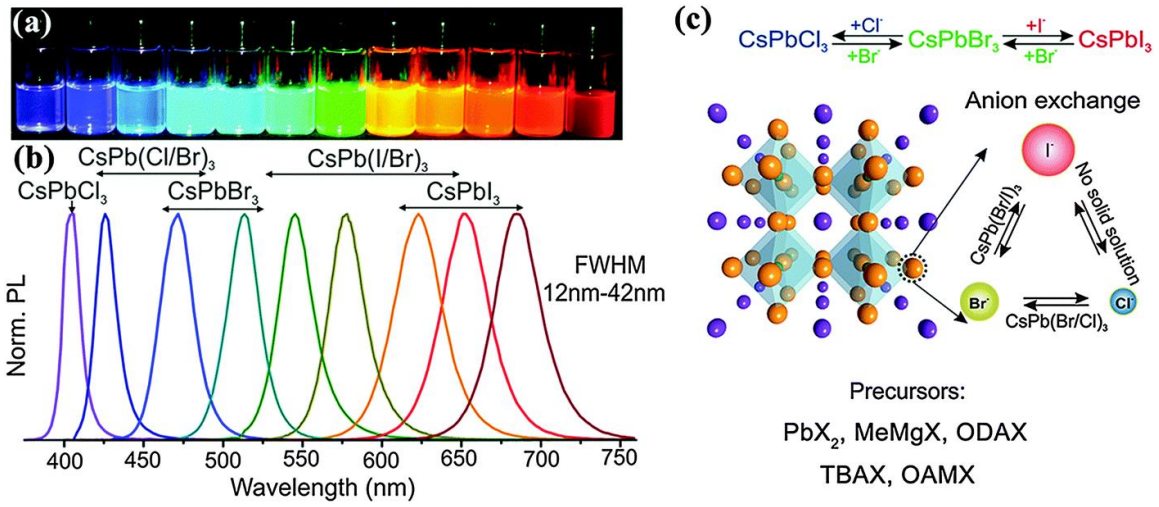

Fig. 4: (a) Image of all inorganic $CsPbX_3$ perovskite NC colloidal solutions in toluene under a UV (365 nm) lamp (b) The representative PL spectra (excited by 400 nm light but 350 nm for $CsPbCl_3$)[42] (c) Schematic of the halide anion-exchange process and suitable reagents used for the reaction[43].

III. Photoluminescence quantum efficiency

Photoluminescence quantum efficiency, is defined as the ratio of the number of converted photon to absorbed photon. High quantum efficiency usually indicates that most of the absorbed photons are converted through radiative recombination processes rather than non-radiative recombination processes. Because of their large absorption coefficient and high quantum efficiency perovskites are considered as excellent light emitters[43]. In both all-inorganic $CsPbX_3$ and organic-inorganic methylammonium lead halide perovskite nanocrystals there has been reported high quantum efficiency up to 90%, without any further surface treatment[37,42]. Whereas, in conventional semiconductors, their nanocrystals suffer from surface defect states or donor-acceptor levels which considerably reduces the quantum efficiency. The high quantum efficiency in perovskite is the result of clear bandgap with negligible charge-trapping states, which greatly promote the exciton radiative recombination efficiency[44]. With high quantum efficiency, perovskites are promising candidates for many optoelectronic applications including lasing, light emitting diode, etc..

IV. Quantum confinement effect

If the size of a semiconductor is small enough to be compared to Bohr radius of excitons, quantum confinement can be observed on the optical properties of the semiconductor. Excitons are confined in all three spatial dimensions, which results in a transition from continuous to discrete energy levels. Therefore, the optical absorption and emission properties can be tuned by changing the size of the semiconductor. Quantum confinement effect is associated with nanocrystals and it results in the blue shift of the bandgap with the decrease of the size. In all-inorganic $CsPbBr_3$ perovskite nanocrystals, the exciton Bohr radius is calculated to be 7 nm, quantum confinement effect is quite outstanding in $CsPbBr_3$ perovskite nanocrystals when its size becomes comparable with the exciton Bohr radius. It is possible to tune the emission of $CsPbBr_3$ perovskite nanocrystals from around 2.7 eV to 2.4 eV with the size changing from 4 nm to 12 nm as shown in Fig. 5a. Similarly, quantum confinement effect is also observed nanoplates[45] and nanowires[46]. Quantum confinement effect opens a way to tune the emission of semiconductors, which provides the potential use in various light emitting applications.

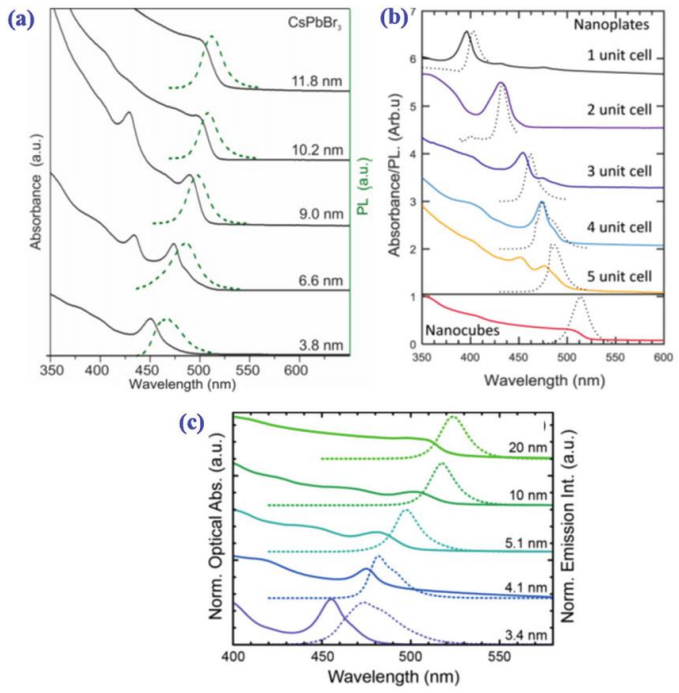

Fig. 5: Quantum confinement effects: UV-vis absorption (solid lines) and emission (dashed lines) spectra of $CsPbBr_3$ (a) NCs with different sizes[42] (b) nanoplates with five different thicknesses and nanocubes[45] (c) nanowires with different widths[46].

1.1.2 Applications of perovskites

Since the first report of using perovskite material in solar cells in 2009[25], perovskites have been extensively studied and have found application in various optoelectronic devices. Metal halide perovskites are emerging as one of the most promising material for light emitting diode due to their easy preparation, low cost, and high performance. An important advantage of perovskites in LED application is that they usually have high color purity with full width half maximum of ~15-25 nm for the electroluminescence spectra. Another advantage is their color tunability in the whole visible spectrum by simply changing the composition of different halides within the compounds. Because of the discovery of amplified spontaneous emission (ASE) in perovskites[16], many researches have put effort to explore their potential applications in laser technology. Among the first to use perovskite as gain medium was Deschler F. et al.[47]. Also, low dimensional perovskites are being tackled in many other optoelectronic applications such as FET[48], photodetector[49], and single photon emitter[50].

1.1.3 Limitations of Perovskites

Even though perovskites, as mentioned above, have extraordinary properties they face many challenges with respect to their stability, limiting their use in large-scale practical application and industrialization. Perovskites, are vulnerable and tend to decompose in ambient air for various reasons, there is a great number of studies that aim to understand the factors that are involved and also the mechanisms that lay behind them. Water, and as a consequence humidity in the air, is one of the major causes of perovskites instability[51]. Water molecules react with $[PbX_6]^{4-}$ octahedral units, which leads to broken bonds between the cation Cs^+ and the $[PbX_6]^{4-}$ octahedra[52]. $[PbX_6]^{4-}$ octahedra also transform into $[PbBr_8]^{6-}$ hendecahedral units and with increasing water content that turn into PbX_2. At the same time, defects such as vacancies in perovskites, have high affinity to water as well as oxygen molecules and their absorption can accelerate perovskite degradation through the vacancy-assisted decomposition mechanism[53]. Meanwhile, due to the ionic nature, lead halide perovskites are soluble and degradable in almost all polar organic solvents. Fig. 6 shows the effect of polar solvents on crude solutions of as-synthesized $CsPbBr_3$ nanocrystals. The solvents of dimethyl sulfoxide, dimethylformamide, methanol and ethanol have destructive effect to $CsPbBr_3$, leading to the loss of their optical properties. In addition, perovskites are sensitive to temperature and light irradiation. The crystal phases of the perovskite are temperature-dependent, as mentioned above perovskites exist in more than one phase, by treating the material with different temperature

a phase change is possible which leads to the modification of the optoelectronic properties of the material. With continuous light irradiation perovskites degrade, especially with UV, blue and white light[54,55]. With increasing irradiation time there is an increase in the photoluminescence intensity due to aggregation of nanocrystals and the formation of Pb^0 clusters[56].

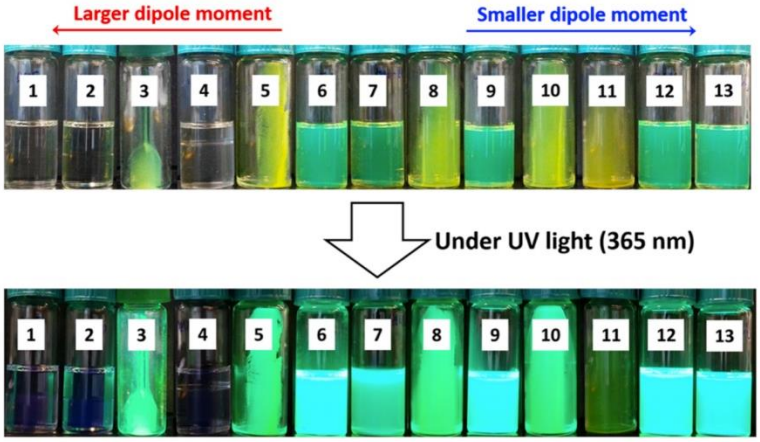

Fig. 6: Effect of polar solvents on crude solutions of $CsPbBr_3$ nanocrystals. Solvents arranged in order of increasing dipole moment: (1) dimethyl sulfoxide, (2) dimethylformamide, (3) acetonitrile, (4) methanol, (5) acetone, (6) ethyl acetate, (7) tert-butanol, (8) 1-butanol, (9) tetrahydrofuran, (10) isopropyl alcohol, (11) ethanol, (12) chloroform, and (13) dichloromethane, respectively[57].

Furthermore, the known toxicity of lead has aroused serious environmental and health related concerns[58].

1.1.4 Perovskite incorporation to host material

In order to improve the stability of perovskite nanocrystals (PNCs) while at the same time minimizing environmental and health concerns, various strategies have been implemented, such as surface modification[59] or the incorporation within host materials. For example, organic polymers have been used as promising hosts material for the incorporation of perovskite crystals. In particular polymethyl methacrylate (PMMA)[60], polystyrene (PS)[61], and poly(styrene-ethylene-butylene-styrene) (SEBS)[62] have been employed. Even though the encapsulation in polymers enhances PNCs stability, it is only for a short period of time because of degradation and aging of the polymer itself. At the same time, because of their poor thermal stability, polymer compounds limit significantly the application in high power devices. Finally, upon the incorporation of PNCs within organic

polymers, significant spectral shifts and reduction in the photoluminescence (PL) features are induced[63].

On the other hand, due to their chemical and thermal strength, inorganic oxide glasses seem to resolve the preceding limitations, while offering remarkable PL stability of the embedded PNCs[64-78]. In addition, because of their high transparency in most of the visible range the emission feature of the encapsulated PNCs is almost unaffected. Glasses are relatively easy to make and at the same time non-toxic making them candidate for handling material. So far, there are two main methods for the encapsulation of PNCs within glass matrices. The most common one involves the simultaneous melting of both perovskite and glass precursors[64-78]. Following the typical quenching for the formation of the glass, the growth of PNCs is achieved by means of additional annealing treatments[64-76], or by laser-assisted crystallization techniques[77,78] plus conventional annealing treatments[79]. The use of a femtosecond laser for the precipitation of the PV in the glass matrix allows the crystallization of the PV in a specific location as shown in Fig.7a. At the same time, it gives the opportunity of reversible PV crystallization, at which the crystallization of the perovskite occurs through the femtosecond laser and then the recovery happens via annealing treatment, as shown in Fig. 7b.[78]

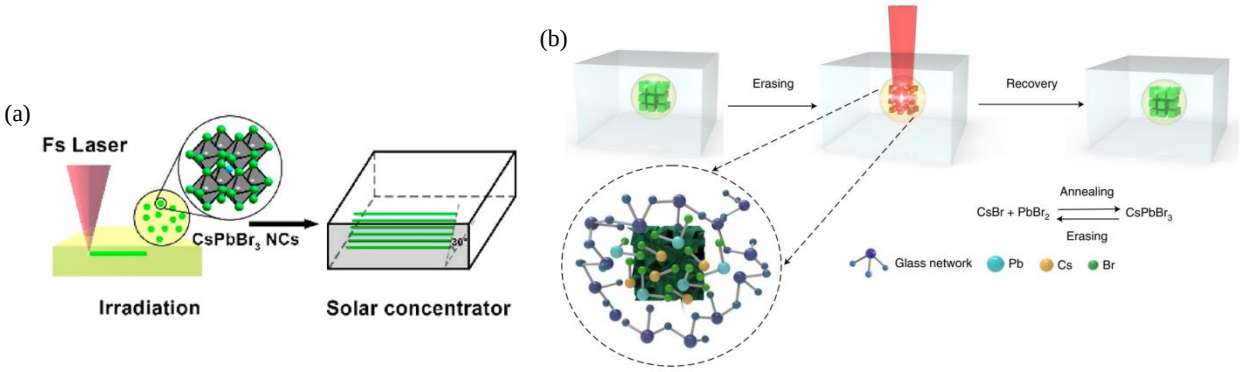

Fig. 7: (a) Schematic illustration of fs-laser-irradiation-induced precipitation of $CsPbBr_3$ perovskite NCs in glass.[77] (b) Proposed mechanisms of the reversible formation and decomposition of $CsPbBr_3$ QDs.[78]

A recently developed alternative approach for the synthesis of PV-Glasses involves the low-temperature, post-glass melting encapsulation of previously prepared PNCs within transparent inorganic oxide glass[80], the fabrication procedure is shown in Fig. 8. Namely, the as prepared PNCs are incorporated within the glass substrate following heat treatments at temperature near the glass transition temperature (T_g) of the glass, i.e. around 160 ^oC. These methods offer remarkable

advantages in terms of the development of highly photoluminescence perovskite-based materials of superior stability, while rendering the formation of perovskite periodic patterns feasible.

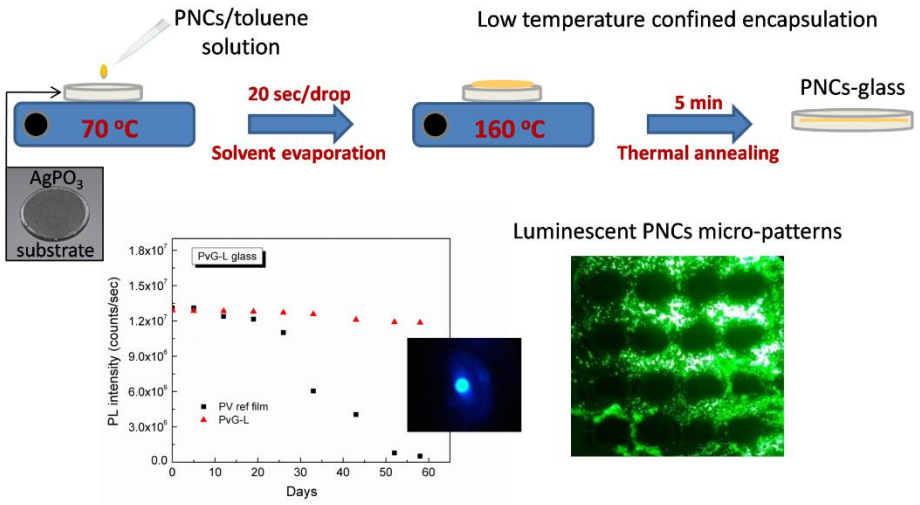

Fig. 8: (a) Schematic animation of the fabrication procedure of PvG-L (layered perovskite sample) and PvG-C (clustered perovskite sample) perovskite glasses. (b) Percentage of PL intensity versus days of exposure to air (see text). (c) Fluorescence photos of micro-dotted optical textures encapsulated within PvG-L glass after laser patterning with horizontal separation steps (see text) of 400 μm.[80]

1.2 Glasses and the glassy state

1.2.1 The nature of glass and glass transition temperature

Glasses are considered to be amorphous solids, in which the atoms are not organized in a periodic lattice pattern like crystals are. Glasses appear to be solid-like in appearance, also there thermal and mechanical properties are similar to those of the corresponding crystals. Although, they do not have a sharp, well-defined melting point as do crystals. Unlike crystals, physical properties of glasses are isotropic, a characteristic that makes glasses resemble liquids. Inferentially, glasses are non-crystalline solids.

In order to achieve glass formation, the process of crystallization must be bypassed. Crystallization can occur if there are sufficiently large number of nuclei present in the mass, and if a large enough crystal growth rate follows. For the crystallization of the material to be avoided, rapid cooling must

be implemented. All materials can be prepared as non-crystalline solids by rapid cooling, however the cooling rate varies from material to material. Contemplate, a small amount of material in high temperature that is in liquid form. This state is given by point a in the V-T diagram (Fig. 9). In the V-T diagram the behavior of amorphous material, from liquid to solid, is plotted. The temperature is plotted in the x-axis and the volume/enthalpy occupied by the material is plotted along the y-axis, where temperature T_m is the melting point, and T_g is the glass transition temperature. When a glass is made, the liquid is quickly cooled from a supercooled liquid, an intermediate state between liquid and glass. In order for the material to become an amorphous solid it has to be cooled in a temperature below the glass transition temperature (T_g). Past this point, the molecular movement of the material's atoms has slowed and the material forms a glass[81-83]. This formed amorphous solid, is more organized compared to a liquid and at the same time it is less organized than a crystal.

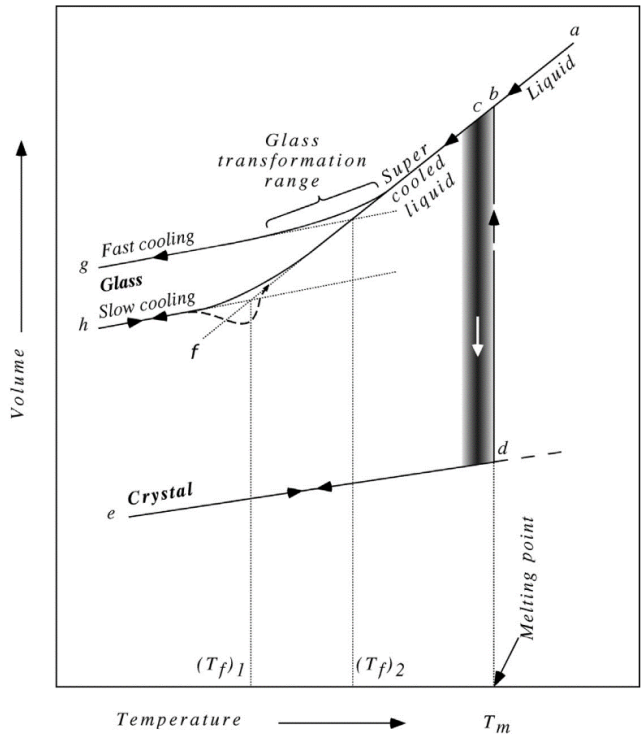

Fig. 9: Volume-Temperature diagram on the glass formation of a liquid.[84]

If the liquid passes the melting point T_m and crystallization doesn't occur, the liquid moves to a supercooled liquid form. When further cooling, a temperature is reached at which molecules, rearrange so slowly that they cannot sufficiently reach equilibrium configurations on a time scale that is allowed by the cooling rate. This leads, to a frozen structure of the melt, and the resulting material is glass. Unlike the melting temperature T_m the glass transition temperature T_g isn't as well

defined. Because there is no discontinuous change in any of the physical properties of the material the glass transition is not considered to be a usual phase transition. When cooling, if the cooling rate is reduced it leads to a shift of the T_g to lower temperature. Also, the T_g changes with starting material chosen for the composition. When the temperature becomes lower than the T_g, the liquid rearranges itself into a lower volume and the molecules become less and less mobile, which leads to an increase of the viscosity of the system. The range of glass formation is represented by the temperatures $(T_f)_1$ and $(T_f)_2$, $(T_f)_1$ represents a glass formed by a reduced cooling rate (slow cooling) and $(T_f)_2$ a glass with an increased cooling rate (fast cooling) which has a lower density than the slow cooled glass[84].

1.2.2 Oxide Glasses

The most widely used glasses are oxide glasses, mainly formed from the following network former oxides SiO_2, P_2O_5, B_2O_3, GeO_2, TeO_2, As_2O_3, Sb_2O_3, Al_2O_3 etc. The basic molecular structural units that form the glass matrix depend on the type of network former. As for instance, in borate glasses these are both BO_4 tetrahedra and BO_3 triangles, and in telluride glasses very distorted tetrahedra. Oxide glasses, can be developed through a number of different techniques such as the sol-gel route and chemical vapor deposition, although the easiest way to obtain a glass is via the melt-quenching technique.

In order to determine the structure of oxide glasses there is the Continuous Random Network model that was presented in a classical paper by Zachariasen[85]. He argued that since the mechanical properties of glasses are similar to those of the corresponding crystals, the atomic forces in both must be of the same order but with a variation in the number of structural units and the periodicity of lattice. Due to the randomness of the glass network, glasses have higher internal energy of the corresponding crystals. This difference, is believed to be, by Zachariasen, small resulting that glass should have an open and flexible structure. Both crystalline and glassy forms are composed of AO_3 triangles that are joined to each other at corners, the difference between the glass and the corresponding crystal is that a disorder is introduced in the A-O-A angles called bond angle and slight changes in the A-O bond length. He laid down four rules for glass formation in a compound A_mO_n.

i. An oxygen atom is linked to no more than two atoms of A.
ii. The oxygen coordination around A is small, say 3 or 4.

iii. The cation polyhedral share corners, not edges, not faces.
iv. At least three corners are shared.

Zachariasen therefore defined a glass as a "substance" that can form extended three-dimensional networks lacking periodicity with energy content comparable with that of the corresponding crystal network.

In order to be able to understand the processes that occur in glasses, it is needed to understand their structure. Glass components are classified as either glass network formers (NWFs) or glass network modifiers (NWMs). To form a stable glass, network formers are the main component, this is because they form the backbone of the network. Common NWFs in oxides glasses are SiO_2, GeO_2, B_2O_3, Al_2O_3 and P_2O_5. These components create a structural unit with connectivity provided by the oxygen atoms. By using only network formers, it is possible to develop a stable glass without adding any other component. Most common, inorganic network glasses are silicates such as window glasses. The basic structural unit of the silicate glass network is a tetrahedron, in which the silicon atom is surrounded by four oxygens. The tetrahedra, connected by bridging oxygens, are randomly oriented in space because they have been "frozen" into place by rapid quenching.

The second category of glass components is network modifiers. They change the bond characteristics, although they aren't capable of participating to the network of the system. Most common modifiers in oxide glasses are alkali oxides (e.g., Li_2O, Na_2O, and K_2O) and alkaline earth oxides (e.g., MgO, CaO, SrO, and BaO). The glass is modified by conversion of the bridging oxygens to non-bridging oxygens leading to a reduced connectivity of the network[84].

1.2.3 Properties of Glasses

Because glasses can be developed from different starting material this means that the end product can have different properties. Despite, the elastic and strength behavior of the glasses, almost all other of their properties are sensitive to the chemical composition, in other words to the atomic structure. In oxide glasses, the chemical composition, atomic structure and property relationships are based upon the following:

1. the coordination number of the network forming ion
2. the connectivity of the structure, which is determined by the nonbridging oxygens, that are determined by both the nature and concentration of network modifying ions

3. the openness of the structure, determined by the concentration of network modifying ions
4. the mobility of the network modifying ions

So, comparing two different systems, the silicates which are tetrahedrally connected networks, and borates that are triangularly connected networks, the first one is more viscous. When having glass networks in which the interspatial spaces have less network modifying ions, they are characterized by lower density. In oxide glasses, alkali ions are used commonly as network modifiers, and they are the most mobile species through interspatial, the higher the alkali concentration, the lower the chemical durability and electrical resistivity of the material.

Phosphate glasses can be used for a variety of applications within very diverse fields, in most cases a proper combination of several of their properties is needed, which can be formed through the development of complex compositions. The starting material of phosphate salts, for the development of phosphate glasses differ and depend on the end product, some examples are: $(NH_4)_2HPO_4$, P_2O_5, $NH_4H_2PO_4$, etc. Boric oxide (B_2O_3), used in borate glasses, is an important oxide because it adds properties to the glass that otherwise would be impossible to obtain. It is considered to be the component that has the higher glass forming tendency, this is because it's impossible for the molten B_2O_3 to form a crystal on its own[86].

The optical properties of a material determine how it will interact with light. When light travels through a medium, a part of it is reflected from the front surface, a part is absorbed, and the remainder is transmitted. Concerning glasses there are two key features that make them valuable material and these are that they can be worked into different shapes and the fact that they are transparent to the visible region. At wavelengths smaller than visible light, electrons have enough energy to interact with the glass. Strong absorption bands arise from the electron excitations and produce a UV-cutoff resulting to most glasses being opaque in the UV. These excitations are of two types:

1. Intrinsic excitation at which electrons are excited from the valence band to unoccupied states in the exciton or the conduction band levels
2. Intra-ionic transition at which the transfer of an electron occurs between the shells of an ion to the shells of a neighboring ion.

Because in this study we examine the photoluminescence properties of the perovskite nanocrystals it is important that the host material is transparent in the visible spectrum. Fig. 10 shows the optical absorbance spectra of two of the three glasses used, at which it can be seen that in most of the visible range there is almost no absorption.

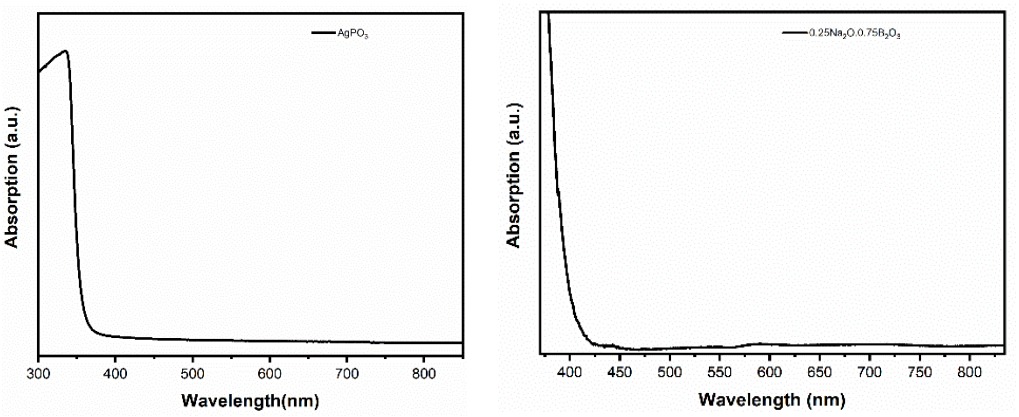

Fig. 10: Optical absorbance spectra of pristine (a) $AgPO_3$ glass and (b) $0.25Na_2O$-$0.75B_2O_3$ glasses[87].

1.2.4 Synthesis of glasses

Most common glass development route is via the melt-quenching technique[88]. This process consists of the mixing of raw materials, batch melting at high temperatures and fining. Additional steps to this process can be the fining step at which bubbles are removed from the melt by either making them rise physically to the surface or by addition of fining agents and thermal annealing of the as-prepared glass in order to release thermal stress. Glasses can also be manufactured from gels, using the alkoxide route[89]. The first step consists of hydrolysis and condensation of alkoxides and additional metals in organic solvents. The obtained gel is then dried, densified and sintered. High-homogeneity and high-purity glasses are obtainable by the sol-gel route. Disadvantages of the sol-gel process include high cost as well as long processing times and also it is difficult to produce large fragments. Moreover, chemical vapor deposition (CVD) may be used in order to obtain glass films[90]. In a typical CVD, the substrate is exposed to volatile precursors, which react on the substrate surface and produce the desired deposit. Glass fibers can be formed at high temperatures using a bulk preformed rod.

1.2.5 Applications of glasses

Glasses are one of the most versatile material, leading to their use in a very wide range applications from everyday use objects to highly sophisticated applications. Most widely seen application of

glasses are the windows, which are silicate glasses. Regarding their first electronic application they were used in xerography[91] and electrostatic imaging. Comparing glasses to their corresponding crystal, they have lower electrical conductivity and this is because their structural disorder hinders the motion of the charged carriers that make the electrical current, making glasses electrical insulators. Thermal conductivity is as well lower than that of the corresponding crystals, making glasses goof thermal insulators. Furthermore, the continuous liquid-to-solid transition near the glass transition temperature is connected to classical applications of glasses. Their ability to viscosity tunability of the melt makes it conveniently processed into desirable shapes, glass blowing being the most widely known example of this. Glasses, also find application in medicine, the discovery of mesoporous bioactive glasses reveal new application in the fields of bone regeneration[92] and drug delivery systems[93]. Glasses can also be used in optoelectronic devices. Optics is the scientific field concerned with the emission, absorption, polarization, reflection, refraction and diffraction of light, and the use of devices that depend on one or more of these phenomena. Glasses are one of the most important material used in optics since their first use in optical technology, this can be pointed to the invention of telescopes. Since then a great amount of applications have been established, such as their use in linear integrated optical devises (waveguides)[94], in nonlinear optical devises[95], glasses for lasers (amplifying media, optical switches, lenses, windows lights and substrates), functional glasses such as electrochromic[96], photochromic[97] and photosensitive[98] glasses, etc..

Aim of the thesis

2.1 Problem statement & aim of thesis

So far, the effect of the perovskite nanocrystals (PNCs) incorporation procedure on the development and properties of the so-formed PV-Glasses has been explored in detail[64-78]. Rather differently, there is still significant luck on understanding the effect of the selected glass composition and network type on PNCs-glass network interactions, and thus, on the outcome of the synthesis. At the same time, it has not been investigated in detail, what are the chemical interactions when introducing the perovskite precursors into the melting procedure. In inorganic oxide glasses, the network former structural units connect with each other through bridging oxygens, while the amount of terminal oxygen are modified by the quantity of network modifier components. As mentioned above, the addition of network modifiers into the glass system reduces the connectivity of the network, creating network gaps. For example, it has been seen that upon the introduction of lead atoms to the glass system the perovskite precursors lead atoms can be found both bonded to oxygen atoms and at the same time they can exist as free atoms within the network gaps[72]. It is only the free atoms that can contribute to the formation of the perovskite inside the glass. At the same time, the necessity of annealing procedures has also been established for the perovskite crystallization. By applying additional post-glass melting heat treatments, the structure of the network becomes less stiff and gives the opportunity of movement to the atoms which they can now form perovskite crystalline compounds.

In this work, aiming to shed light on the effect of the host glass matrix on the properties of the composite PV-glasses, we explore the formation of cesium lead bromide and cesium lead iodide PNCs within three types of inorganic oxide glasses. Namely, starting from the 'soft' low glass transition (T_g) temperature silver metaphosphate ($AgPO_3$) glass, going on to a double network former silver borophosphate (xAg_2O-yP_2O_5-zB_2O_3), and finally to the more rigid sodium borate glass ($0.25Na_2O$-$0.75B_2O_3$). The selection of these glass families was made for two main reasons. First, to investigate the effect of silver nanoparticles presence on the chemistry of the formation of PNCs within the glass. Second, for the investigation of the effect of the glass network type on the growth of PNCs.

Experimental Part: Material & Methods

3.1 Materials

High purity chemical were used in the form of powder, $AgNO_3$(99.9999%), $NH_4H_2PO_4$(99.999%), B_2O_3(99.98%), Na_2CO_3(99.999%), Cs_2CO_3(99.994%), $PbBr_2$(99.999%), NaBr(99.99%), PbI_2(99,9985%), AgI(99.999%), chemicals were supplied from Acros Organics, Alfa Aesar and Silga Aldrich.

3.2 Development of Perovskite-Glasses

3.2.1 Melt quenching technique

All glasses were developed through conventional melt quenching technique upon mixing and melting together appropriate amounts of the reagents[87] For the perovskite (PV) phosphate glass family, glasses with nominal composition 0.1PV-0.9$AgPO_3$ were prepared, upon mixing together dry powders of $AgNO_3$, $NH_4H_2PO_4$, Cs_2CO_3, $PbBr_2$, NaBr, PbI_2, and AgI. Fig. 11 presents a schematic representation of the glass melting and quenching procedure, followed by typical annealing treatments for thermal crystallization. Along similar lines, borophosphate system glasses with nominal composition of 0.1PV-0.9(0.5Ag_2O-0.3B_2O_3-0.2P_2O_5) were synthesized upon melting the previous reagents and the proper amount of B_2O_3. Finally, composite sodium borate-based PV-Glasses with nominal compositions of 0.05PV-0.95(0.25Na_2O-0.75B_2O_3) and 0.1PV-0.9(0.25Na_2O-0.75B_2O_3) were prepared upon melting the previously mentioned reagents upon replacing $AgNO_3$ and $NH_4H_2PO_4$ with the appropriate stoichiometric amounts of Na_2CO_3 and B_2O_3. The precursors for each glass were mixed thoroughly in a platinum crucible, and melted in an electrical furnace at 450-1100 ^oC for 30 min. Following splat quenching for the development of glass specimens, additional annealing treatments were performed to induce chemical interactions between the perovskite components and the formation of PNCs. As it will be discussed in the following sections, the annealing temperature was varied in accordance with the nature of each composite glass system.

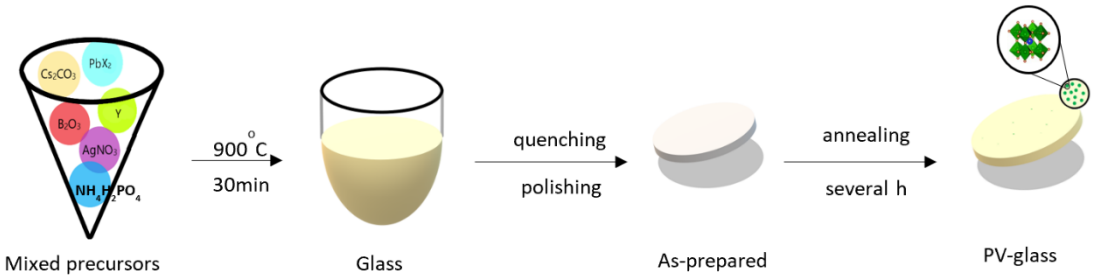

Fig. 11: Schematic illustration of the glass preparation and annealing for the crystallization of $CsPbX_3$ perovskite NCs in glass[87].

3.3 Characterization of the Glass and Perovskite-Glass samples

3.3.1 Scanning electron microscopy (SEM)

Scanning electron microscope (SEM) is a type of microscope that uses an electron beam to illuminate the specimen and produce a magnified image. The beam of electrons is produced at the top of the microscope (electron gun), follows a vertical path through the column of the microscope, makes its way through electromagnetic lenses which focus and directs the beam down towards the sample. The beam passes through pairs of scanning coils or pairs of deflector plates in the electron column, typically in the final lens, which deflect the beam in the x and y axes so that it scans over a rectangular area of the sample surface. The focused beam of high-energy electrons generates a variety of signals at the surface of solid specimens. The signals that derive from electron-sample interactions reveal information about the sample, including external morphology or surface topography, chemical composition and other properties, such as electrical conductivity. The spatial resolution of SEM depends on the size of the electron spot, which in turn depends on both the wavelength of the electrons and the electron-optical system which produces the scanning beam. Depending on the instrument, the resolution ranges between 1 and 20 nm.

Glass surfaces were morphologically characterized by scanning electron microscopy (SEM). SEM was performed on a JEOL 7000 field emission scanning electron microscope with an acceleration voltage of 15 kV.

3.3.2 Raman spectroscopy

Raman spectroscopy is associated with the investigation of bond vibrations and gives information on the chemical structure. Monochromatic light is used to irradiate the sample and the scattered light from the sample is the one observed. If the irradiation frequency is v_o and the light scattered from the sample is of frequence v_o we have Rayleigh scattering. Although, there is a small fraction of light that does not have frequency v_o and has a frequency of v_i. Raman scattering is the process that produces light with frequency of v_i. The difference Iv_o-v_iI is the energy absorbed by the sample. In the case of $v_i<v_o$ we have Stokes radiation, whereas, for $v_i>v_o$ we have Anti-Stokes radiation.

A Nicolet Almega XR Micro Raman analysis system equipped with a diode-pumped solid-state laser (DPSS) was used for the perovskite glass characterization. Excitation wavelength was set to 473nm. The system consists of a confocal single monochromator spectrometer and utilizes a scanning motorized stage to move around the sample of interest. A 100x Olympus objective lens (with numerical aperture of 0.9) is included for tight focus and data collection in micrometer resolution. Max output power was measured 50mW and controlled via a neutral density filter. The signal is analyzed by a high-resolution grating (2400 lines per mm).

3.3.3 Photoluminescence spectroscopy

Photoluminescence spectroscopy is a non-destructive technique used for the characterization of the electronic and optical properties of matter. Photoluminescence is the light emission (luminescence) of matter that follows the absorption of electromagnetic radiation, due to the initiation of the process by photos, the prefix photo- is used. The photo-excitation causes the material to jump to a higher electronic state, and will then release energy, as it relaxes and returns back to a lower energy level. The emission of light or luminescence through this process is photoluminescence, PL.

The spectra were collected in a backscattering setup shown in Fig 12. The setup was used to capture micro-photoluminescence (-PL) spectra. A SuperK EVO supercontinuum white light source (NKT Photonics) was combined with a SuperK Varia (NKT Photonics) grating to allow for wavelength selection. The selected wavelengths were 470nm and 543nm. The PL signal was analyzed using an iHR-320 spectrometer (Horiba Scientific/Jobin Yvon Technology) in this arrangement. It's a 320mm focal length (f/4.1 aperture) automated spectrometer with two separate gratings on its turret: 300g/mm and 1200g/mm. The monochromator's exit is equipped with a Syncerity

multichannel charge-coupled device (CCD) Deep Cooled Camera. A Mitutoyo 50x (NA:0.42, f=200mm) focuses down to ~1μm the spot size for the sample excitation.

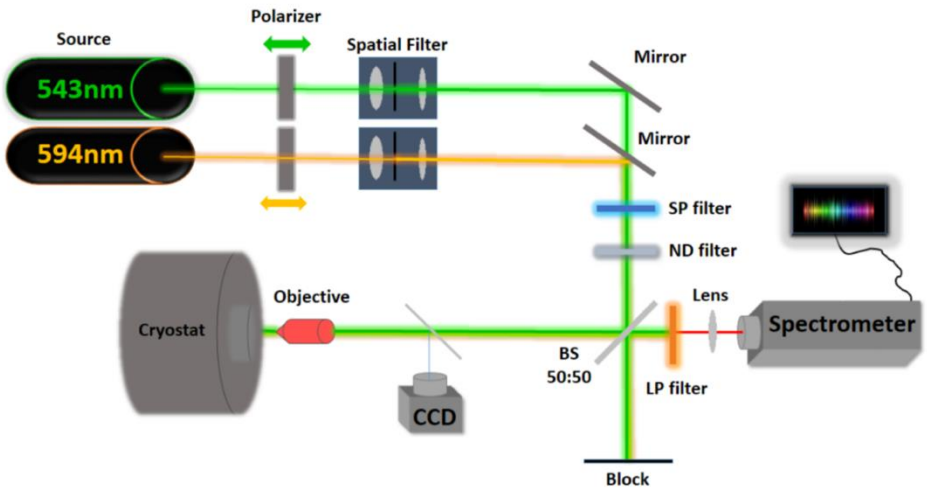

Fig. 12: Schematic representation of the μ-PL configuration[99].

3.3.4 X-Ray Diffractometer (XRD)

The crystal structure of the fabricated perovskites glasses were studied by an X-Ray Rigaku (RINT-2000) Diffractometer operating with a continuous scan of Cu Ka1 radiation with $\lambda = 1.54056$ Å. All XRD measurements were performed with a scan rate of $0.1^{o}/s$ in the range of $2\theta = 20^{o} - 80^{o}$.

3.3.5 Transmission Electron Microscopy (TEM)

Transmission electron microscope (TEM) is a type of microscope that uses a beam of electrons to visualize specimens and thus produce a highly magnified image. As like SEM, TEM uses an electron gun at the top to emit electrons. The beam is focused by an electromagnetic lens into a very fine beam, that then passes through the sample. Electrons are either scattered or hit a fluorescence screen in the bottom of the microscope. An image of the sample with its assorted parts shown in different shades according to its density appears on the screen.

Transmission electron microscopy images were obtained by a TEM JEOL 2010 equipped with a LaB6 type emission gun at a voltage of 160 kV.

3.3.6 Ultraviolet-Visible Spectroscopy (UV-Vis)

UV-Vis spectroscopy is an analytical technique that measures the amount of discrete wavelengths of UV or visible light that are absorbed by a sample.

A PerkinElmer UV/vis (Lambda 950) spectrometer was used to measure the absorption of the developed PV-Glasses over the wavelength range of 280−860nm.

Results and discussion

4.1 Composite Perovskite Silver Phosphate Glasses

For the perovskite (PV) phosphate glass family, glasses with nominal composition 0.1PV-0.9$AgPO_3$ were prepared, as well as the pristine silver phosphate glass ($AgPO_3$). Figs. 13a and b present scanning electron microscopy (SEM) surface photos of the perovskite glasses 0.1$CsPbBr_3$-0.9$AgPO_3$ and 0.1$CsPbI_3$-0.9$AgPO_3$, respectively. As expected, the incorporation of the perovskite precursors within the phosphate glass do not cause any visible structural modification on the surface of both samples.

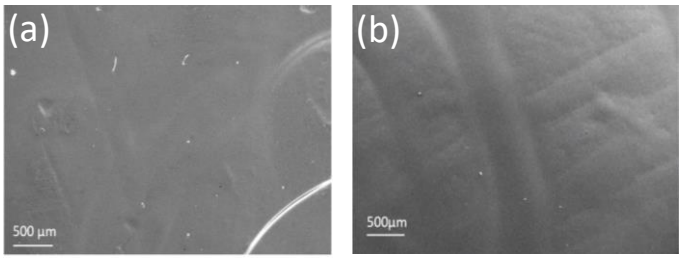

Fig. 13: Scanning electron microscopy (SEM) images of the surface of 0.1$CsPbBr_3$-0.9$AgPO_3$ (a) and 0.1$CsPbI_3$-0.9$AgPO_3$ (b) glasses.

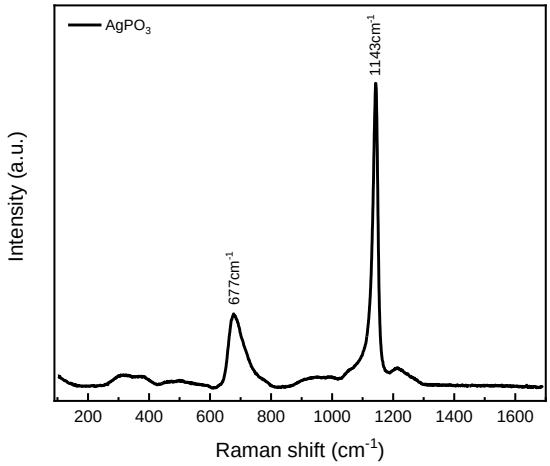

Fig. 14: Normalized room temperature Raman spectra of the pristine $AgPO_3$ glass.

Raman spectroscopy was employed in order to investigate any structural modifications of the phosphate glass network upon mixing and melting together the PV precursors. Fig. 14 shows the room temperature Raman spectra of the pristine $AgPO_3$ glass. The metaphosphate network of the $AgPO_3$ glass consists mainly of polymer-like chains which are formed by connected phosphate tetrahedral units having two bridging (Ø) and two non-bridging (O) oxygen atoms $(PØ_2O_2)^-$ [100-103]. The strongest Raman band at ca. 1140 cm^{-1} arises from the symmetric stretching vibration of terminal PO^{2-} entities, $\nu_{(s)}(PO^{2-})$, of the network, whereas the broader feature at ca. 670 cm^{-1} is attributed to the symmetric stretching movement of the P-O-P bridges within the phosphate backbone, $\nu_{(s)}$(P-O-P).

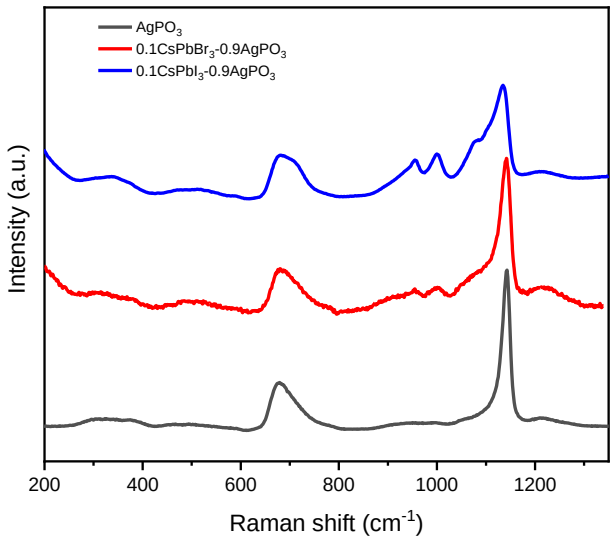

Fig. 15: Normalized room temperature Raman spectra of the pristine $AgPO_3$ glass, the perovskite glasses $0.1CsPbBr_3$-$0.9AgPO_3$ and $0.1CsPbI_3$-$0.9AgPO_3$, respectively.

Fig. 15, shows the room temperature Raman spectra of the two composite glasses, along with the corresponding spectrum of the pristine silver phosphate glass. With a closer look at the spectra, it can be seen that the incorporation of the perovskite precursors introduces a strong shoulder at ca. 1090 cm^{-1}, and two more features at 1000 cm^{-1} and 950 cm^{-1}. The shoulder at 1090 cm^{-1} originates from the asymmetric vibration of pyrophosphate entities, $\nu_{(as)}(PO_3^{2-})$, while the mode at 1000 cm^{-1} is assigned to the corresponding symmetric vibration of the same units, $\nu_{(s)}(PO_3^{2-})$ [100-103]. The band at ca. 950 cm^{-1} is attributed to the presence of orthophosphate units, $\nu(PO_4^{3-})$, within the glass matrix [100-103]. These spectroscopic findings imply that both lead salts ($PbBr_2$, and PbI_2), react with the phosphate glass network upon heating, for the formation of orthophosphate lead species, $Pb_3(PO_4)_2$.

Moreover, the appearance of the characteristic Raman features at 950 cm^{-1} and 1000 cm^{-1} for the two PV-Glasses implies one more modification on the metaphosphate glass network at which there is a more cross-linked pyrophosphate, that has more terminal phosphate units. Additional evidence on this observation comes from the relative intensities of the two dominant Raman bands at ca. 670 cm^{-1} and 1140 cm^{-1}. The relative intensities of these Raman signatures provide immediate indication of the population of terminal or bridging phosphate units, so the change in the intensity of the bands means change on the population. Notably, the intensity of the latter band relative to the former decreases for the PV-Glasses, indicating the creation of more non-bridging (terminal) oxygen atoms throughout the phosphate network. Inevitably, as the lead salts react with the network, the stoichiometry is spoiled, and the cations of the remaining PV precursors act as network modifiers, i.e. charge balancing the negative charge of non-bridging oxygens.

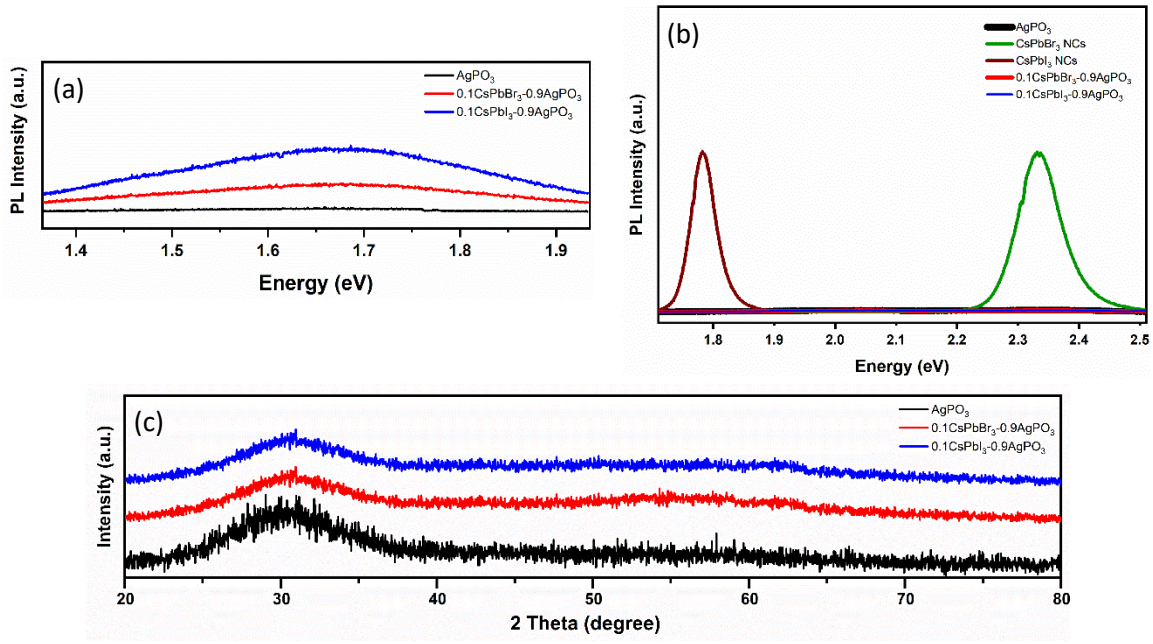

Fig. 16: (a), (b) Room temperature photoluminescence (PL) spectra, for the sake of comparison the PL spectra of the non-encapsulated PV NCs are added in (b) and (c) XRD patterns of pristine $AgPO_3$ glass and the PV-Glasses[87].

Fig. 16a, b demonstrates the photoluminescence (PL) spectra for both composite glasses as well as the pristine silver phosphate glass[87]. The latter figure depicts also the PL spectra of the non-encapsulated $CsPbBr_3$ and $CsPbI_3$ PNCs for the sake of comparison. Notably, all glasses exhibit no PL emission, which based on the above is not surprising. In case of the formation of perovskite nanocrystals with bromine and iodine halogens the perovskite glasses would exhibit PL emission at 2.35 eV and 1.78 eV respectively[64,74].

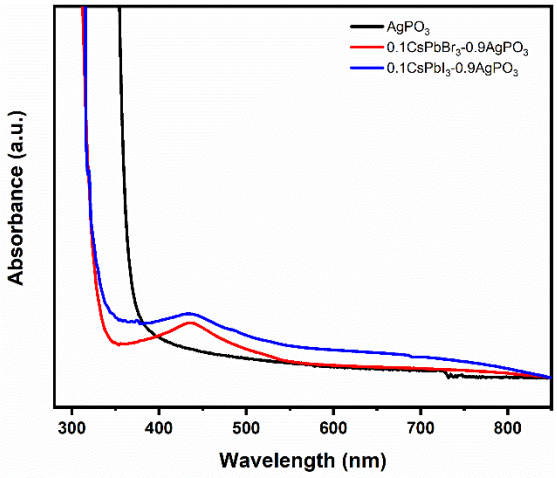

Fig. 17: Optical absorbance spectra of pristine $AgPO_3$ glass and composite glasses.

Moreover, the corresponding absorbance profiles of the pristine $AgPO_3$ glass and the two composite glasses are presented in Fig. 17. Inspection of Fig. 17 reveals that the composite glasses, on the contrary to the pristine $AgPO_3$ glass, exhibit distinct absorption features at 420-450 nm which are attributed to the presence of silver nanoparticles (AgNPs)[104,105] following the annealing treatments. Notably, in these glasses there is no evidence of the characteristic absorption of perovskite NCs in the visible range[74].

At the same time, the corresponding XRD patterns presented in Fig. 16c demonstrate the absence of crystalline phase, leading to the conclusion that there is no perovskite formation in the glass matrix, data that support the above. At the same time the crystallization of PNCs within this glass system is also significantly hindered by another factor. Silver phosphates glass transition temperature (T_g) is of 192^{o}C[106]**.** In order to have perovskite crystallization in a glass, the glass substrate containing the perovskite precursors undergoes annealing treatment in temperature near the T_g of the glass. During the post-melting annealing treatment of the PV-Glasses at temperatures near and above the T_g, the phosphate network gains viscosity and becomes active for interactions with the perovskite precursors. Thus, prior to any PV crystal growth which requires extensive thermal treatment for several hours, the PV precursors react with the host phosphate network, and they become unavailable for the formation of PNCs within the glass matrix. By understanding the chemical interactions of the silver phosphate glass with the perovskite precursors, we can move on to the next glass host that will have higher T_g so that perovskite crystallization could be possible.

4.2 Composite Perovskite Silver Borophosphate Glasses

As said above a low glass transition temperature hinders the crystallization of the perovskite in the glass matrix, so in order to overcome this obstacle a second network former is added to the silver phosphate glass. By the addition of B_2O_3 to the glass system we have the synthesis of PV-Glasses with nominal composition $0.1CsPbI_3$-$0.9(0.5Ag_2O$-$0.3B_2O_3$-$0.2P_2O_5)$ samples were annealed at 320°C for 1-3h. The T_g of the pristine mixed-former host silver-borophosphate glass is 350 °C[107,108] as shown in the literature**.** Fig. 18a shows a photo of the $0.1CsPbI_3$-$0.9(0.5Ag_2O$-$0.3B_2O_3$-$0.2P_2O_5)$ glass sample without annealing treatment, while Fig. 18b shows an indicative photo after 3 hours of annealing at 320°C. It becomes apparent that the heat treatment induces a metallic nature of the glass. The corresponding room temperature PL spectra are shown in Fig. 18c. Likewise to what observed for the phosphate single-network system (Fig. 16a, b), the composite borophosphate glass exhibits only broad fluorescence features arising from the agglomeration of metallic silver nanoparticles (AgNPs)[106,109,110]**,** which has been observed to intensively occur upon heating silver-containing phosphate glasses near T_g[106,109,110].

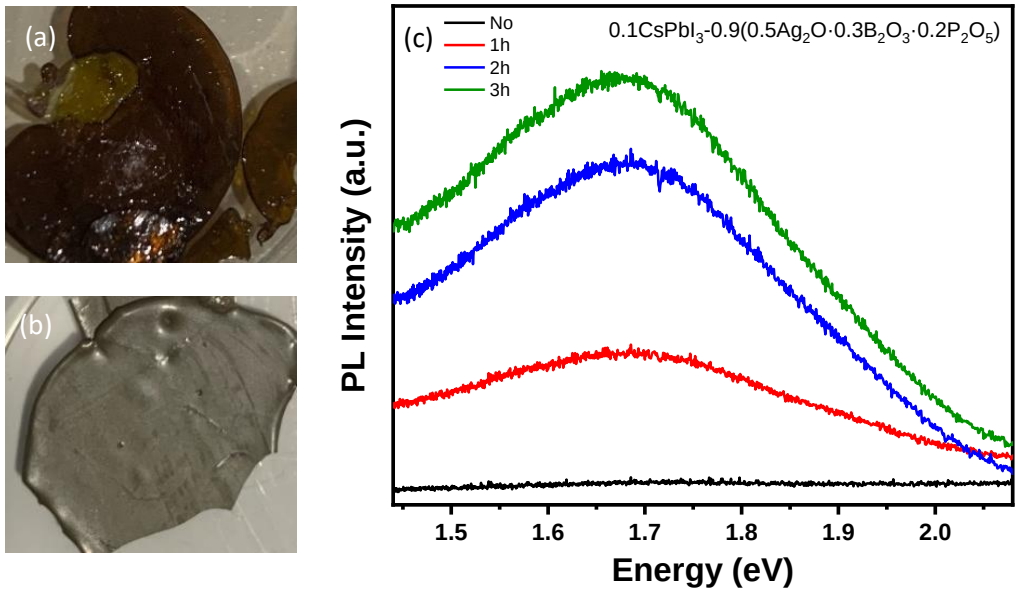

Fig. 18: Pictures of (a) $0.1CsPbI_3$-$0.9(0.5Ag_2O$-$0.3B_2O_3$-$0.2P_2O_5)$ composite glass after quenching, and (b) after 3 hours of annealing at 320 °C. (c) Indicative room temperature photoluminescence (PL) spectra[87].

4.3 Composite Perovskite Sodium Borate Glasses

The last composite system of the present study consists of silver-free sodium borate glasses ($0.25Na_2O$-$0.75B_2O_3$) in order to avoid silver agglomeration upon heat treatment[87]. In this glass system, sodium cations act as the network modifiers of the borate glass network. Glasses of nominal composition $0.05CsPbBr_3$-$0.95(0.25Na_2O$-$0.75B_2O_3)$ and $0.1CsPbBr_3$-$0.9(0.25Na_2O$-$0.75B_2O_3)$ were developed and the as-prepared glasses were annealed for 10h at temperatures 600, 700, 800^oC. Figs. 19a and b present room temperature photoluminescence spectra of $0.05CsPbBr_3$-$0.95(0.25Na_2O$-$0.75B_2O_3)$ and $0.1CsPbBr_3$-$0.9(0.25Na_2O$-$0.75B_2O_3)$ glasses, respectively, annealed for 10 hours at 700^oC. The inset of Fig. 19a shows a photo of the $0.05CsPbBr_3$-$0.95(0.25Na_2O$-$0.75B_2O_3)$ glass under UV light exposure, from which it is possible to see that there is slight emission, this is a first indication of perovskite crystallization inside the host glass. As seen in the PL spectra, both PV-Sodium Borate glasses exhibit double peak emission profiles at the vicinity of 1.8 eV. Recently, it was demonstrated that the often observed double peak PL spectra of perovskite crystals originates from an extensive self-absorption effect, which is amplified by the high internal reflection within the crystal[111,112]. It is observed that for all samples, the emission structured consists of two peaks, the dominant at higher energy and a weaker (shoulder) at lower energy level. Especially, for the samples $0.05CsPbBr_3$-$0.95(0.25Na_2O$-$0.75B_2O_3)$ and $0.1CsPbBr_3$-$0.9(0.25Na_2O$-$0.75B_2O_3)$, the dominant higher energy level peak arises at 1.83 eV is the main emission directly outcoupled from the crystals, while the lower energy band arises at 1.79 eV and is attributed to additional emission upon multiple internal reflection and self-absorption phenomena[111,112].

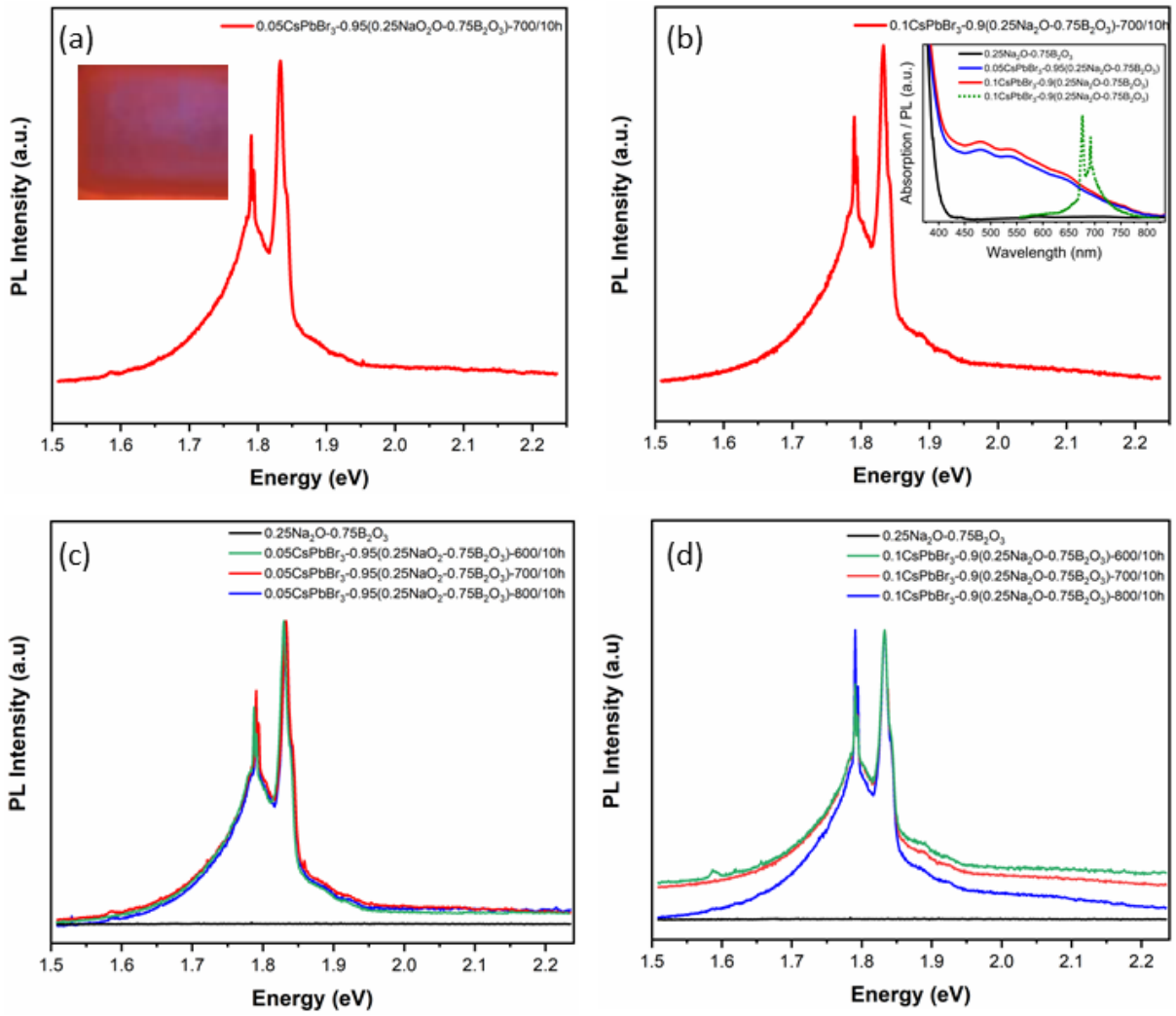

Fig. 19: Room temperature photoluminescence (PL) spectra of (a) 0.05CsPbBr$_3$-0.95(0.25Na$_2$O-0.75B$_2$O$_3$), and (b) 0.1CsPbBr$_3$-0.9(0.25Na$_2$O-0.75B$_2$O$_3$) composite glasses after 10 hours of annealing at 700^{o}C. The inset of (a) show a picture of the former glass under UV light irradiation. The inset of (b) depicts the corresponding optical absorbance profiles of the composite PV-Glasses and the pristine sodium borate glass, while the PL of the 0.1CsPbBr$_3$ PV-Glass is also included. PL spectra of (c) 0.05CsPbBr$_3$-0.95(0.25Na$_2$O-0.75B$_2$O$_3$), and (d) 0.1CsPbBr$_3$-0.9(0.25Na$_2$O-0.75B$_2$O$_3$) composite glasses after 10 hours of annealing at various temperatures (600, 700, 800^{o}C). The corresponding spectra of the pristine 0.25Na$_2$O-0.75B$_2$O$_3$ glass is also shown at both spectra[87].

Fig. 19c shows the PL profiles of additional 0.05CsPbBr$_3$-0.95(0.25Na$_2$O-0.75B$_2$O$_3$) samples annealed for the same period of time, at temperatures 600^{o}C and 800^{o}C, whereas the corresponding spectrum of the pristine 0.25Na$_2$O-0.75B$_2$O$_3$ host glass is also shown for the sake of comparison. The pristine 0.25Na$_2$O-0.75B$_2$O$_3$ host glass exhibits no photoluminescence emission, proving that the observed PL features of the composite PV-Glasses arise from the crystallization of PNCs. As seen from the spectra, the exact same double band PL profile is exhibited for all samples

independently of the annealing temperature. This implies that the reduction or increase of stresses within the host borate glass network upon annealing treatments at higher and lower temperatures, leaves the PL properties of the PNCs unaffected and as a consequence the perovskites crystals as well. Leading to the conclusion that the obtained double peak PL profile arises only from within the PNCs without any coupling with the borate backbone. On the contrary, the concentration of PNCs affects the relative intensities of the PL bands, particularly for the higher annealing temperatures. Fig. 19d, shows the PL spectra of the three $0.1CsPbBr_3$-$0.9(0.25Na_2O$-$0.75B_2O_3$ glasses annealed at various temperatures. There is a significant enhancement of the 1.79 eV lower energy band noticed when compared to the main PL feature at 1.83 eV, implying an enhancement of the self-absorption and internal reflection features when the amount of PNCs is doubled within the host glass matrix.

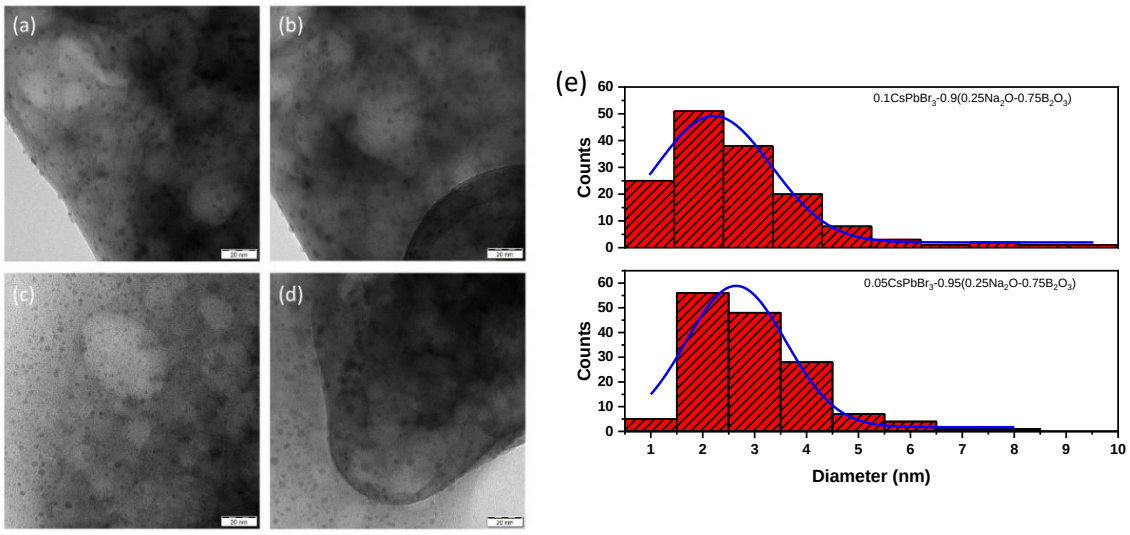

Fig. 20: Transmission electron microscopy (TEM) images of cesium lead bromide PNCs within $0.05CsPbBr_3$-$0.95(0.25Na_2O$-$0.75B_2O_3)$ glass (a and b), and within $0.1CsPbBr_3$-$0.1(0.25Na_2O$-$0.75B_2O_3)$ glass (c and d). (e) Histograms of PNCs size distribution in PV-Glasses[87].

Figs. 20a and b show the transmission electron microscopy (TEM) images of $0.05CsPbBr_3$-$0.95(0.25Na_2O$-$0.75B_2O_3)$ glass, while Figs. 20c and d show the corresponding photos of the $0.1CsPbBr_3$-$0.9(0.25Na_2O$-$0.75B_2O_3)$ sample. The examination of TEM images reveals that the $CsPbBr_3$ nanocrystals diameter of ranges from 2 to 10 nm[87]. Fig. 20e shows the histograms of PNCs size distribution in PV-Glasses. And as seen the average value of size for both composite glasses is of 2-3 nm. Also, as can be seen the concentration increase of PNCs within the glass

matrix leaves the diameter of the PNCs unaffected. Although, as expected, by the increase of the concentration of the perovskite in the glass matrix there is a decrease in the distance between the so-formed PNCs.

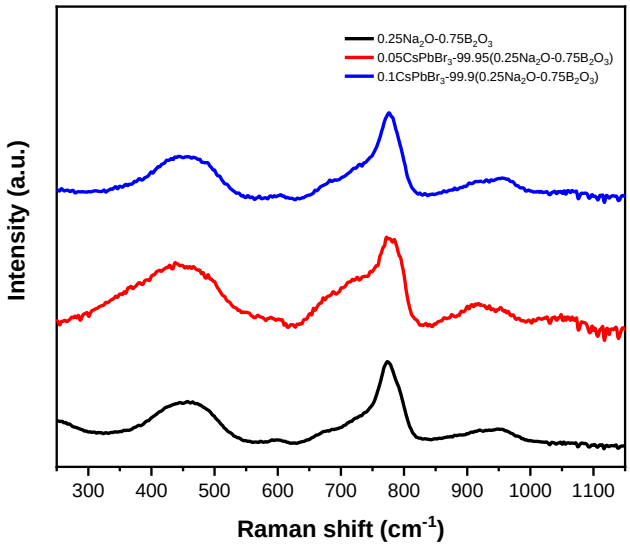

Fig. 21. Room temperature Raman spectra of the two composite PV-Glasses and the pristine $0.25Na_2O$-$0.75B_2O_3$ glass[87].

Raman spectroscopy was employed in order to investigate the interaction of the perovskite nanocrystals with the sodium borate glass network. Fig. 21 shows the room temperature Raman spectra of the pristine sodium borate glass and the two PV-Glasses. All three spectra are dominated by two main features, namely a key band at ca. 790 cm^{-1} which originates from the symmetric vibration of the boroxol ring, and a broader profile at ca. 450 cm^{-1} that is attributed to isolated diborate groups[113]. Compared with the spectra of the pristine glass, the spectra oφ the perovskite glasses exhibit an enhancement of the Raman modes at the vicinity of 700-735 cm^{-1}. These Raman modes are attributed to the symmetric vibration of metaborate chains[113] of the borate network. So, it is revealed that the growth of PNCs within the glass by means of annealing treatments results to the partial breaking of boroxol rings leading to the formation of numerous chains that are terminated with negatively charged non-bridging oxygen atoms.

As shown above, the main PL band was obtained considerably redshifted at 1.83 eV (Fig. 19), compared with the typically expected that is at the vicinity of 2.36 eV[64-69,74,80]. The creation of negatively charged non-bridging oxygen atoms upon perovskite formation provides a probable explanation for the obtained redshift of the PL features for both $CsPbBr_3$ composite PV-Glasses[87] Based on the literature, in perovskite compounds of the ABX_3 form, the cation A^+ plays a minor

role on the energy bandgap of the crystal. Although, the bandgap is strongly influenced by the anion halide X^- as well as the nature of the bond B-X[42,114,115]. Namely, the modification of the halide anion changes the distance and possibly the angle of the X-Pb-X bonds within the PbX_6 octahedral of the perovskite structure. In the case of inorganic lead halide perovskites, the bandgap progressively decreases from Cl to Br to I, this is directly related to the smaller electronegativity and larger bond angles of the larger halide atom[42,114,115]. Because of the crystallization of the perovskite nanocrystals in the glass matrix, negatively charged non-bridging oxygen are formed, making the so-formed PNCs surrounded by them. Because there is no cation modifier to balance this negative charge, this additional negative charge could strongly reduce the electronegativity of the Br-Pb-Br bonds, and by this causing a decrease in the bandgap energy of the encapsulated PNCs[87].

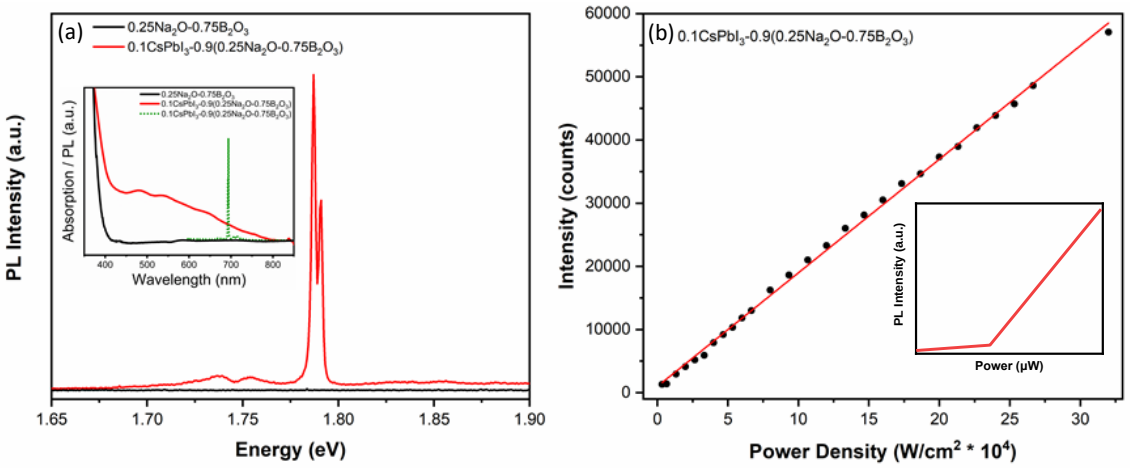

Fig. 22. (a) Room temperature photoluminescence (PL) spectra of $0.1CsPbI_3$-$0.9(0.25Na_2O$-$0.75B_2O_3)$ composite glass after 8 hours of annealing at 700 °C. The inset of (a) shows the corresponding optical absorbance profiles of the composite $CsPbI_3$ PV-Glass and the pristine sodium borate glass, while the PL of the former is also included. (b) Power excitation density dependence of the PL intensity. The inset of (b) shows the PL intensity dependence on the excitation power of a lasing system[87].

Finally, Fig. 22a depicts the photoluminescence spectrum of $0.1CsPbI_3$-$0.1(0.25Na_2O$-$0.75B_2O_3)$ composite glass[87]. The main PL feature at 1.78 eV dominates, while the two considerably weaker bands attributed to self-absorption and internal reflections within the PNCs are observed at 1.73 and 1.76 eV. Unlike the $CsPbBr_3$ PV-Glass, the $CsPbI_3$ PV-Glass exhibits the PL feature exactly to the reported energy level[42,74]. This implies that in case of $CsPbI_3$ the energy bandgap of the encapsulated PNCs remains mostly unaffected from the environment of the host glass network. This finding is rationalized in terms of the fact that the I-Pb-I bonds within the perovskite octahedral will be considerably less vulnerable to the possible presence of additional non-bridging negatively

charged entities, because of I atom low electronegativity of the I, i.e. the less electronegative anion of all found in all-inorganic PNCs. The final part of this study, was to investigate whether the so-formed $CsPbI_3$-based PV-Glass exhibit random laser behavior. Fig. 22b presents the PL intensity dependence on the excitation power of the 473 nm laser. A linear dependence is revealed, suggesting that lasing features are absent from this PV-Glass architecture. The inset of Fig. 22b shows the expected photoluminescence intensity dependance on the excitation power if the system had lasing properties. It is believed that the self-absorption and internal reflection phenomena prohibit the lasing effect. This linear dependence of the PL intensity to the power density is expected for exhitonic transitions.

The findings of this study show the role of employing extra network former additives of high coordination number on the development of composite inorganic oxide PV-Glasses[64-74], typical examples of such compounds are Sb_2O_3 and, $Zn(PO_3)_2$. So far, the reasons behind the use of such glass forming components, is the creation of more cross-linked, rigid, and expanded host glass network, that will offer a suitable platform for annealing treatments at higher temperatures, that so far are known to favor the growth of PNCs[87]. Notably, the significance of free space and volume within the glass matrix on assisting ion movement has been thoroughly studied[116]. Thus, the expansion of glass network upon employing formers of high coordination ability facilitates further the perovskite growth procedures within glasses upon improving ionic movement. Nevertheless, the findings of the present study highlight another important role of the highly coordinated additives. That is to assist on maintaining the high connectivity of the network and minimize the formation of chain terminal units with negatively charged oxygens that will consequently alter the optical and luminescence properties of the incorporated perovskite nanocrystals. On the other hand, single-network former glass systems like the borate of this study, may offer an advanced platform for controllably tailoring the optical properties by means of the intentional introduction of negatively charged terminal units, that is without the need to change the composition of the perovskite itself.

Conclusions

We have explored the formation of all-inorganic lead halide PNCs within three different types of inorganic oxide glasses. Firstly, it was attempted to grow PNCs inside silver metaphosphate glass ($AgPO_3$), a glass characterized by its 'soft' phosphate backbone glass network and a low glass transition temperature (T_g). While the low T_g appears promising on reducing the fabrication cost, it becomes an obstacle for the PNCs crystallization, because it limits dramatically the temperature range of the post-melting annealing treatment which is essential for the perovskite crystal growth. At the same time, as seen the phosphate network is vulnerable under chemical reactions with the lead precursor salts leading to the formation of orthophosphate lead species, $Pb_3(PO_4)_2$. In order to overcome these limitations, the study moves on to the investigation of the borophosphate glass family which exhibit higher T_g and network connectivity. In this case, the metallic nature of the glass due to the high concentration of silver was negative on PNCs formation upon annealing treatments at elevated temperatures. The final part of this study, was focused on the development of silver-free sodium borate composite PV-Glasses. The developed composite glasses exhibit interesting photoluminescent properties due to the incorporated PNCs. In the case of $CsPbBr_3$ composite glasses, we saw a significant redshift of the photoluminescence emission profile obtained, this was because of the interaction of the PNCs with the negatively charged oxygen atoms of the borate glass network. These charged oxygen atoms arise from the breaking of the borate rings of the network upon PNCs growth within the glass. The last composition investigated was the $CsPbI_3$ composite PV-Glasses of the same host matrix. $CsPbI_3$-glasses exhibit considerably less tuning of the PL band, due to the lower electronegativity of the iodine atom when compared to bromine.

References

1. R. J. Sutton et al., Bandgap-Tunable Cesium Lead Halide Perovskites with High Thermal Stability for Efficient Solar Cells, Adv. Energy Mater. 2016, 6, 1502458
2. M. Filip, G. Eperon, H. Snaith et al., Steric engineering of metal-halide perovskites with tunable optical band gaps. Nat Commun 5, 5757 (2014).
3. J. D. Roo et al., Highly Dynamic Ligand Binding and Light Absorption Coefficient of Cesium Lead Bromide Perovskite Nanocrystals, ACS Nano 2016, 10, 2071−2081
4. W. S. Yang et al., High-performance photovoltaic perovskite layers fabricated through intramolecular exchange, Science, 348, 1234, 2015
5. C. Wehrenfennig et al., High Charge Carrier Mobilities and Lifetimes in Organolead Trihalide Perovskites, Adv. Mater. 2014, 26, 1584–1589
6. D. Shi et al., Low trap-state density and long carrier diffusion in organolead trihalide perovskite single crystals, Science, 347, 519, 2015
7. M.V. Kovalenko et al., Properties and potential optoelectronic application of lead halide perovskite nanocrystals, Science 358 (6364) (2017) 745–750
8. C.C. Stoumpos et al., Halide perovskites: poor man's high-performance semiconductors, Adv. Mater. 28 (28) (2016) 5778–5793
9. L. Pedesseau et al., Advances and promises of layered halide hybrid perovskite semiconductors, ACS Nano 10 (11) (2016) 9776–9786
10. Y. Xu et al., Research progress on the stability of all inorganic $CsPbX_3$ perovskites nanocrystals, J. Liaocheng Univ.(Nat. Sci. Edi.) 32 (1) (2019) 69–80
11. P. Qin et al., Inorganic hole conductor-based lead halide perovskite solar cells with 12.4% conversion efficiency, Nat Commun 5, 3834 (2014).
12. J. F. Christians et al., An Inorganic Hole Conductor for Organo-Lead Halide Perovskite Solar Cells. Improved Hole Conductivity with Copper Iodide, J. Am. Chem. Soc. 2014, 136, 2, 758–764
13. S. Lee et al., Solar-harvesting lead halide perovskite for artificial photosynthesis, Journal of Energy Chemistry 62 (2021) 11–26
14. L. Zhang et al., Ultra-bright and highly efficient inorganic based perovskite light-emitting diodes, Nat Commun 8, 15640 (2017).
15. H. Cho et al., Overcoming the electroluminescence efficiency limitations of perovskite light-emitting diodes, Science, 350, 1222, 2015
16. G. Xing et al., Low-temperature solution-processed wavelength-tunable perovskites for lasing. Nature materials 13, 476-480, (2014).
17. H. Zhu, et al., Lead halide perovskite nanowire lasers with low lasing thresholds and high quality factors. Nature materials 14, 636-642, (2015).
18. M. Moniruddin et al., Recent progress on perovskite materials in photovoltaic and water splitting applications, Mat. T. Ener. 7 (2018) 246
19. G. Rose (1839) Beschreibung einiger neuer Mineralien vom Ural. Ann der Phys und Chemie 48:551–572
20. D. Weber et al., $CH_3NH_3PbX_3$, ein Pb (II)-System mit kubischer Perowskitstruktur. Z. Naturforsch., J. Chem. Sci. 33, 3, (1978).

21. D. Weber et al., $CH_3NH_3SnBr_xI_{3-x}$ (x = 0-3), ein Sn(II)-System mit kubischer Perowskitstruktur Z. Naturforsch., J. Chem. Sci. 33, 4, (1978).
22. Revolution of Perovskite, Synthesis, Properties and Applications, Narayanasamy Sabari Arul, Vellalapalayam Devaraj Nithya
23. Q. A. Akkerman et al., Nearly Monodisperse Insulator Cs_4PbX_6 (X = Cl, Br, I) Nanocrystals, Their Mixed Halide Compositions, and Their Transformation into $CsPbX_3$ Nanocrystals. Nano Letters, 17(3), 1924, 2017
24. Y. Zhao, K. Zhu, et al., Organic-inorganic hybrid lead halide perovskites for optoelectronic and electronic applications. Chemical Society reviews 45, 655- 689, (2016).
25. A. Kojima et al., Organometal halide perovskites as visible-light sensitizers for photovoltaic cells. *Journal of the American Chemical Society* 131, 6050-6051, (2009).
26. https://www.edinst.com/phase-transitions-halide-perovskite/
27. D. Malyshkin et al., New phase transition in $CsPbBr_3$. Materials Letters, 278, 2020, [128458].
28. S. Hirotsu et al., Structural Phase Transitions in $CsPbBr_3$, J. Phys. Soc. Jpn., 1974, 37, 1393–1398.
29. N. Elumalai et al., Perovskite Solar Cells: Progress and Advancements. Energies, 9(11), 861, 2016
30. A. Walsh & G. W. Watson et al., The origin of the stereochemically active Pb(II) lone pair: DFT calculations on PbO and PbS. J Solid State Chem 178, 1422- 1428, (2005).
31. S. Olthof et al., Research Update: The electronic structure of hybrid perovskite layers and their energetic alignment in devices. APL Materials, 4(9), 091502, (2016).
32. T. Paul et al., Tunable cathodoluminescence over the entire visible window from all-inorganic perovskite $CsPbX_3$ 1D architecture. Journal of Materials Chemistry C, 6(13), 3322, (2018)
33. W. J. Yin et al., Halide perovskite materials for solar cells: a theoretical review. J Mater Chem A 3, 8926-8942, (2015).
34. Q. Wang et al., Doped hole transport layer for efficiency enhancement in planar heterojunction organolead trihalide perovskite solar cells. *Nano Energy* 15, 275-280, (2015).
35. W. L. Hong et al., Efficient Low- Temperature Solution- Processed Lead- Free Perovskite Infrared Light- Emitting Diodes. Advanced materials, (2016).
36. S.A. Veldhuis et al. Perovskite Materials for Light- Emitting Diodes and Lasers. Advanced materials, (2016).
37. K. Lin, J. Xing ,L. N. Quan et al., Perovskite light-emitting diodes with external quantum efficiency exceeding 20 per cent. Nature 562, 245–248 (2018)
38. M. Yuan, L. Quan, R. Comin et al., Perovskite energy funnels for efficient light-emitting diodes. Nature Nanotech 11, 872–877 (2016).
39. Y. Tong et al., Highly Luminescent Cesium Lead Halide Perovskite Nanocrystals with Tunable Composition and Thickness by Ultrasonication, Angew. Chem. Int. Ed. 2016, 55, 1 – 7
40. A. Swarnkar et al., Quantum dot-induced phase stabilization of -$CsPbI_3$ perovskite for high-efficiency photovoltaics. Science, 354 (6308), 92, (2016).
41. Y. Fu et al., Nanowire lasers of formamidinium lead halide perovskites and their stabilized alloys with improved stability. Nano letters 16, 1000-1008, (2016).
42. L. Protesescu et al., Nanocrystals of Cesium Lead Halide Perovskites ($CsPbX_3$, X = Cl, Br, and I): Novel Optoelectronic Materials Showing Bright Emission with Wide Color Gamut, Nano Lett., 2015, 15, 3692–3696
43. G. Nedelcu et al., Fast Anion-Exchange in Highly Luminescent Nanocrystals of Cesium Lead Halide Perovskites ($CsPbX_3$, X = Cl, Br, I) Nano Lett., 2015, 15, 5635–5640
44. K. Wu et al., Ultrafast interfacial electron and hole transfer from $CsPbBr_3$ perovskite quantum dots. Journal of the American Chemical Society 137, 12792-12795, (2015).

45. Y. Bekenstein et al., Highly Luminescent Colloidal Nanoplates of Perovskite Cesium Lead Halide and Their Oriented Assemblies J. Am. Chem. Soc. 2015, 137, 16008.
46. M. Imran et al., Colloidal Synthesis of Strongly Fluorescent $CsPbBr_3$ Nanowires with Width Tunable down to the Quantum Confinement Regime Chem. Mater. 2016, 28, 6450.
47. F. Deschler et al., High Photoluminescence Efficiency and Optically Pumped Lasing in Solution-Processed Mixed Halide Perovskite Semiconductors. J Phys Chem Lett 5, 1421-1426, (2014).
48. J. Y. Liu et al., Two-Dimensional $CH_3NH_3Pbl_3$ Perovskite: Synthesis and Optoelectronic Application. Acs Nano 10, 3536-3542, (2016).
49. H. Deng et al., Growth, patterning and alignment of organolead iodide perovskite nanowires for optoelectronic devices. Nanoscale 7, 4163-4170, (2015).
50. Y. S. Park et al., Room Temperature Single-Photon Emission from Individual Perovskite Quantum Dots. Acs Nano 9, 10386-10393, (2015).
51. Z. Zhu et al., Metal halide perovskites: stability and sensing-ability, J. Mater. Chem. C, 6, 10121-10137 (2018)
52. M. Liu et al., Unveiling solvent-related effect on phase transformations in $CsBr–PbBr_2$ system: coordination and ratio of precursors, Chem. Mater. 30 (17) (2018) 5846–5852
53. C. Ran et al., Defects in metal triiodide perovskite materials towards high-performance solar cells: origin, impact, characterization, and engineering, Chem. Soc. Rev., 2018, 47, 4581–4610.
54. S. Huang et al., Morphology evolution and degradation of $CsPbBr_3$ nanocrystals under blue light emitting diode illumination, ACS Appl. Mater. Interfaces 9 (8) (2017) 7249–7258
55. R.P. Xu et al., In situ observation of light illumination-induced degradation in organometal mixed-halide perovskite films, ACS Appl. Mater. Interfaces 10 (7) (2018) 6737–6746
56. R. An et al., Photostability and photodegradation processes in colloidal $CsPbI_3$ perovskite quantum dots, ACS Appl. Mater. Interfaces 10 (45) (2018) 39222–39227
57. Y. Kim et al., Efficient Luminescence from Perovskite Quantum Dot Solids. ACS Applied Materials & Interfaces, 7(45), 25007–25013, (2015).
58. R. A. Goyer et al., Lead Toxicity: Current Concerns, Environmental Health Perspectives, 100, 177-187, (1993)
59. Y. Hou et al., Enhanced moisture stability of metal halide perovskite solar cells based on sulfur-oleylamine surface modification, Nanoscale Horiz., 2019, 4, 208-213
60. K. Ma et al., In situ fabrication of halide perovskite nanocrystals embedded in polymer composites via microfluidic spinning microreactors, J. Mater. Chem. C, 5, 9398-9404, (2017)
61. X. Liang et al., Ethanol-Precipitable, Silica-Passivated Perovskite Nanocrystals Incorporated into Polystyrene Microspheres for Long-Term Storage and Reusage, Angew. Chem. 131, 2825 –2829 (2019)
62. S. N. Raja et al., Encapsulation of Perovskite Nanocrystals into Macroscale Polymer Matrices: Enhanced Stability and Polarization, ACS Appl. Mater. Interfaces 8, 35523 (2016)
63. J. H. Cha et al., Nanoscale optical imaging of perovskite nanocrystals directly embedded in polymer fiber, Composites Science and Technology 181 (2019) 107666
64. S. Yuan et al., In Situ Crystallization Synthesis of CsPbBr3 Perovskite Quantum Dots Embedded Glasses with Improved Stability for Solid-State-Lighting and Random Upconverted Lasing, ACS Appl. Mater. Interfaces **10**(22) 18918–18926, (2018)
65. P. Li et al., A new whole family perovskites quantum dots ($CsPbX_3$, X=Cl, Br, I) phosphate glasses with full spectral emissions, J. Alloys. Compd. **817,** 153338–153342, (2020)
66. E. Erol et al., Size-controlled emission of long-time durable $CsPbBr_3$ perovskite quantum dots embedded tellurite glass nanocomposites, Chemical Engineering Journal **401** , 126053, (2020)
67. G. Zheng et al., Phosphor in glass composited with $CsPb(BrI)_3$ perovskite nanocrystals embedded glass for high CRI WLED application, Optik, 248,168097, 2021.

68. Y. Liu et al., Upconversion Luminescence in Yb/Ln (Ln = Er, Tm) Doped Oxyhalide Glasses Containing $CsPbBr_3$ Perovskite Nanocrystals, Journal of the European Ceramic Society, 39, 4275–4282, (2019)
69. Y. Ye et al., Highly Luminescent Cesium Lead Halide Perovskite Nanocrystals Stabilized in Glasses for Light-Emitting Applications, Adv. Optical Mater., 1801663, (2019)
70. Y. Zhu et al., A Cyan Emitting $CsPbBr_3$ Perovskite Quantum Dot Glass with Bi Doping, ECS J. Solid State Sci. Technol., **9,** 126003, (2020)
71. X. Liu et al., Stable, Low-Threshold Amplification Spontaneous Emission of Blue Emitting $CsPbCl_2Br_1$ Perovskite Nanocrystals Glasses with Controlled Crystallization, ACS Photonics 8, 887−893, (2021)
72. B. Yang et al., Component regulation and crystallization mechanism of $CsPbBr_3/Cs_4PbBr_6$ perovskite composite quantum dots-embedded borosilicate glass for light emitting application, Applied Surface Science **512**, 145655, (2020)
73. Y. Du et al., Precipitation of $CsPbBr_3$ Quantum Dots in Borophosphate Glasses Inducted by Heat-treatment and UV-NIR Ultrafast Lasers, Chem. Eng. J. 401, 126132, (2020)
74. D. Chen et al., $CsPbX_3$ (X = Br, I) perovskite quantum dot embedded low-melting phosphosilicate glasses: controllable crystallization, thermal stability and tunable emissions, J. Mater. Chem. C, 6, 6832-6839, (2018)
75. X. Di et al., Use of long-term stable $CsPbBr_3$ perovskite quantum dots in phospho-silicate glass for highly efficient white LEDs, Chem. Commun., **53**, 11068-11071, (2017)
76. Z. Yang et al., One-step precipitated all-inorganic perovskite QDs from amorphous media for backlighting display and reproducible laser-driven white lighting, Chem. Eng. J.,427,131379, (2022)
77. Y. Hu et al., Femtosecond-Laser-Induced Precipitation of $CsPbBr_3$ Perovskite Nanocrystals in Glasses for Solar Spectral Conversion, ACS Appl. Nano Mater. **3,** 850−857 (2020)
78. X. Huang et al., Reversible 3D laser printing of perovskite quantum dots inside a transparent medium. Nat. Photonics 14, 82–88 (2020).
79. X. Huang et al., Three-Dimensional Laser-Assisted Patterning of Blue-Emissive Metal Halide Perovskite Nanocrystals inside a Glass with Switchable Photoluminescence, ACS Nano , 14, 3, 3150–3158 (2020)
80. I. Konidakis et al., Highly luminescent and ultrastable cesium lead bromide perovskite patterns generated in phosphate glass matrices, Nanoscale, **12**, 13697-13707 (2020)
81. Sun, K.-H. (1947). Fundamental condition of glass formation. Journal of the American Ceramic Society, 30(9), 277–281
82. WINTER, A. (1957). Glass Formation. Journal of the American Ceramic Society, 40(2), 54–58
83. UHLMANN, D. R. (1983). Glass Formation, a Contemporary View. Journal of the American Ceramic Society, 66(2), 95–100.
84. Fundamentals of Inorganic Glasses, Arun Varshneya, John Mauro
85. W. H. Zachariasen et al. J. Am. Chem. Soc. 1932, 54, 10, 3841–3851
86. Manfred Eigen, CHAPTER 12 - OXIDE GLASSES, Editor(s): K.J. Rao, Structural Chemistry of Glasses, Elsevier Science Ltd, 2002, Pages 463-511, ISBN 9780080439587
87. A. Karagiannaki et al., Opt. Mater. Express, 2022, accepted.
88. D. Carta et al., The effect of composition on the structure of sodium borophosphate glasses, Journal of Non-Crystalline Solids, Volume 354, Issue 31, 2008, Pages 3671-3677
89. R. Puyan et al., Preparation of silica and soda-silica glasses by sol-gel process, Journal of Non Crystalline Solids 41 (1980) 105-115
90. W. Kern et al., Optimized chemical vapor deposition of borophosphosilicate glass films, RCA Review, Vol. 46, June 1985, 117-152
91. Pfister, G. Electronic properties of chalcogenide glasses and their use in xerography. JEM 8, 789–837 (1979).

92. L. Larry L. et al., Bioactive glasses: Importance of structure and properties in bone regeneration, Journal of Molecular Structure, Volume 1073, 2014, Pages 24-30
93. W. Xia et al., Well-ordered mesoporous bioactive glasses (MBG): A promising bioactive drug delivery system, Journal of Controlled Release, Volume 110, Issue 3, 2006, Pages 522-530
94. J.-F. Viens et al., "Fabrication and Characterization of Integrated Optical Waveguides in Sulfide Chalcogenide Glasses, J. Lightwave Technol. 17, 1184- (1999)
95. A. I. Ekimov et al., (1988). Nonlinear Optics of Semiconductor-Doped Glasses. Physica Status Solidi (b), 150(2), 627–633.
96. P. Cossari, et al., Fully integrated electrochromic-OLED devices for highly transparent smart glasses, J. Mater. Chem. C, 2018,6, 7274-7284
97. D. Levy et al., Applications of the sol-gel process for the preparation of photochromic information-recording materials: synthesis, properties, mechanisms, Journal of Non-Crystalline Solids, Volume 113, Issues 2–3, 1989, Pages 137-145
98. D. Hülsenberg et al., Glasses and glass-ceramics for application in micromechanics. Journal of Non-Crystalline Solids, 129(1-3), 199–205, (1991).
99. Paradisanos, I. (2018). Excitons in atomically thin tungsten disulfide (WS_2) layers. (Doctoral Dissertation) University of Crete, Physic Department, Heraklion, Greece.
100. R.F. Bartholomew “Structrure and preperties of silver phosphate glasses- Infrared and Visible spectra” J. Non-Cryst. Sol. 7, 221-235, (1972).
101. A. Fontana, F. Rossi, C. Armellini, G. Dangelo, G. Tripodo and A. Bartolotta, Philos. Mag. B, 79, 2073 (1999).
102. R. K. Brow “Review: the structure of simple phosphate glasses” Journal of Non-Crystalline Solids 263&264, 1-28, (2000).
103. D. Palles, I. Konidakis, C. P. E. Varsamis and E. I. Kamitsos, “Vibrational spectroscopic and bond valence study of structure and bonding in Al2O3-containing AgI–AgPO3 glasses”, RSC Adv.,6, 16697-16710, (2016).
104. D. A. Klyukin, V. D. Dubrovin, A. S. Pshenova, S. E. Putilin, T. A. Shakhverdov, A. N. Tsypkin, N. V. Nikonorov and A. I. Sidorov, "Formation of luminescent and nonluminescent silver nanoparticles in silicate glasses by near-infrared femtosecond laser pulses and subsequent thermal treatment: the role of halogenides," Opt. Eng. 55, 067101, (2016)
105. A.Zhang, J. Zhang and Y. Fang, "Photoluminescence from colloidal silver nanoparticles", J. of Luminescence, 128, 1635, (2008)
106. A.S. Sarkar, I. Konidakis, I. Demeridou, E. Serpetzoglou, G. Kioseoglou, and E. Stratakis “Robust B-exciton emission at room temperature in few layers of MoS_2:Ag nanoheterojunctions embedded into a glass matrix”, Sci. Rep., 10, 15697, (2020).
107. A. Magistris, G. Chiodelli, and M. Duclot “Silver borophosphate glasses: Ion transport, thermal stability and electrochemical behaviour”, Solid State Ionics, 9-10, 1, 611-615, (1983).
108. S.Kabi, and A.Ghosh “Mixed glass former effect in AgI doped silver borophosphate glasses” Solid State Ionics, 262, 778-781, (2014).
109. I. Konidakis and S. Pissadakis “Optical spectra tuning of all-glass photonic bandgap fiber infiltrated with silver fast-ion-conducting glasses”, Materials, 7, 5736, (2014).
110. I. Konidakis, S. Psilodimitrakopoulos, K. Kosma, A. Lemonis, and E. Stratakis “Effect of composition and temperature on the second harmonic generation of in silver phosphate glasses”, Opt. Mater., 75, 796, (2018).
111. K. Schötz, A.M. Askar, W. Peng, D. Seeberger, T.P. Gujar, M. Thelakkat, A. Köhler, S. Huettner, O.M. Bakr, K. Shankar, and F. Panzer “Double peak emission in lead halide perovskites by self-absorption”, J. Mater. Chem. C, 8, 2289, (2020).
112. Y. Fang , H. Wei , Q. Dong and J. Huang , Quantification of Re-Absorption and Re-Emission Processes to Determine Photon Recycling Efficiency in Perovskite Single Crystals, Nat. Commun., 2017, 8 , 14417

113. A.K. Yadav and P. Singh, “A review of the structures of oxide glasses by Raman spectroscopy”, RSC Adv., 5, 67583, (2015).
114. E.Y. Tiguntseva, G.P. Zograf, F.E. Komissarenko, D.A. Zuev, A.A. Zakhidov, S.V. Makarov, and Y.S. Kivshar “Light emitting halide perovskite nanoantennas”, Nano Lett., 18, 1185, (2018).
115. C.T. Crespo “The effect of the halide anion on the optical properties of lead halide perovskites”, Sol. Energy Mater. Sol. Cells, 195, 269, (2019).
116. M.D. Ingram et al., Significance of activation volumes for cation transport in glassy electrolytes, Phys. Chem. Chem. Phys., 6, 3659, (2004).